Emerald Insight

International Journal of Numerical Methods for Heat & F...

Variational multi-scale finite element approximation of the compressible Navier-Stokes equations
Camilo Andrés Bayona Roa Joan Baiges R Codina

Article information:

To cite this document:
Camilo Andrés Bayona Roa Joan Baiges R Codina , (2016),"Variational multi-scale finite element approximation of the compressible Navier-Stokes equations", International Journal of Numerical Methods for Heat & Fluid Flow, Vol. 26 Iss 3/4 pp. 1240 - 1271
Permanent link to this document:
http://dx.doi.org/10.1108/HFF-11-2015-0483

Downloaded on: 18 May 2016, At: 05:21 (PT)
References: this document contains references to 33 other documents.
To copy this document: permissions@emeraldinsight.com
The fulltext of this document has been downloaded 15 times since 2016*

Access to this document was granted through an Emerald subscription provided by emerald-srm:380560 []

For Authors

If you would like to write for this, or any other Emerald publication, then please use our Emerald for Authors service information about how to choose which publication to write for and submission guidelines are available for all. Please visit www.emeraldinsight.com/authors for more information.

About Emerald www.emeraldinsight.com

Emerald is a global publisher linking research and practice to the benefit of society. The company manages a portfolio of more than 290 journals and over 2,350 books and book series volumes, as well as providing an extensive range of online products and additional customer resources and services.

Emerald is both COUNTER 4 and TRANSFER compliant. The organization is a partner of the Committee on Publication Ethics (COPE) and also works with Portico and the LOCKSS initiative for digital archive preservation.

*Related content and download information correct at time of download.

Downloaded by Kungliga Tekniska Högskolan At 05:21 18 May 2016 (PT)

The current issue and full text archive of this journal is available on Emerald Insight at:
www.emeraldinsight.com/0961-5539.htm

Received 20 November 2015
Revised 25 January 2016
30 January 2016
Accepted 31 January 2016

Downloaded by Kungliga Tekniska Högskolan At 05:21 18 May 2016 (PT)

Variational multi-scale finite element approximation of the compressible Navier-Stokes equations

Camilo Andrés Bayona Roa, Joan Baiges and R. Codina
Centre Internacional de Mètodes Numèrics en Enginyeria (CIMNE), Barcelona, Spain and
Universitat Politécnica de Catalunya, Barcelona, Spain

Abstract

Purpose – The purpose of this paper is to apply the variational multi-scale framework to the finite element approximation of the compressible Navier-Stokes equations written in conservation form. Even though this formulation is relatively well known, some particular features that have been applied with great success in other flow problems are incorporated.

Design/methodology/approach – The orthogonal subgrid scales, the non-linear tracking of these subscales, and their time evolution are applied. Moreover, a systematic way to design the matrix of algorithmic parameters from the perspective of a Fourier analysis is given, and the adjoint of the non-linear operator including the volumetric part of the convective term is defined. Because the subgrid stabilization method works in the streamline direction, an anisotropic shock capturing method that keeps the diffusion unaltered in the direction of the streamlines, but modifies the crosswind diffusion is implemented. The artificial shock capturing diffusivity is calculated by using the orthogonal projection onto the finite element space of the gradient of the solution, instead of the common residual definition. Temporal derivatives are integrated in an explicit fashion.

Findings – Subsonic and supersonic numerical experiments show that including the orthogonal, dynamic, and the non-linear subscales improve the accuracy of the compressible formulation. The non-linearity introduced by the anisotropic shock capturing method has less effect in the convergence behavior to the steady state.

Originality/value – A complete investigation of the stabilized formulation of the compressible problem is addressed.

Keywords Compressible flow, Explicit Runge-Kutta scheme, Shock capturing, Stabilized finite elements, Variational multi-scale (VMS)

Paper type Research paper

1. Introduction

The compressible Navier-Stokes equations are commonly used to model flow problems when compressibility effects become relevant. Some areas that require a compressible flow description are the aerodynamics and aeroacoustics fields, in which applications range from turbo-machinery design to speech therapy. The compressible Navier-Stokes equations consists of the conservation of mass, momentum and energy equations. Thermodynamical properties and constitutive relations of the fluid close the mathematical description. We restrict our problem to perfect fluids in the gas state, which we model using Newton's law for fluids together with the caloric equation, the ideal gas law, and Fourier's heat law. However, other compressible fluids can be modeled by the compressible Navier-Stokes equations using the appropriate constitutive definitions.

International Journal of Numerical Methods for Heat & Fluid Flow
Vol. 26 No. 3/4, 2016
pp. 1240-1271
© Emerald Group Publishing Limited
0961-5539
DOI 10.1108/HFF-11-2015-0483

Downloaded by Kungliga Tekniska Högskolan At 05:21 18 May 2016 (PT)

In this work we are interested in the finite element method (FEM) approximation of compressible flow problems. In particular, we solve this set of equations using the conservative variables formulation, that is, defining density, momentum, and total energy as the problem unknowns. When these equations are approximated by the classical Galerkin approach, numerical instabilities may appear due to the hyperbolic nature of the equations. The first attempt to deal with this instability was the introduction of a stabilizing term into the Galerkin finite element formulation. Within this concept, the Streamline Upwind Petrov Galerkin (SUPG) method by Tezduyar and Hughes (1983) was the first method adopted for solving the compressible Navier-Stokes equations. In that formulation, the authors applied the stabilization methods previously developed for the convection-diffusion equation. The main idea was to optimally introduce numerical diffusion along the streamlines using a stabilization term that contained a matrix of algorithmic parameters, a certain operator applied to the test function, and the residual of the differential equation (e.g. Brooks and Hughes, 1981). An important contribution of this pioneering work was the inclusion of the largest eigenvalue of the hyperbolic system into the matrix of algorithmic parameters. More recently, Polner (2005), Billaud *et al.* (2010), and Sevilla *et al.* (2013) applied the SUPG stabilization into their compressible flow formulations. Some later stabilizations were formulated based on the Galerkin Least Squares method. In all of these works (Shakib, 1989; Hauke and Hughes, 1998; Hauke *et al.*, 2005), the authors transformed the conservative variables into entropy variables using Jacobian transformation matrices.

The multi-scale concept was first included in the compressible Navier-Stokes formulations to account for the effect of the unresolved scales as a turbulence model instead of as a stabilization method. Within this branch, Koobus and Farhat (2004) proposed a mixed formulation that approximated the solution separating a priori the resolved and unresolved turbulent scales. They included the effect of unresolved scales into the solution using a Reynolds stress tensor. The unresolved scales were calculated with a finite volume cell-agglomeration projector. Van Der Bos *et al.* (2007) contrasted that initial work, specifically in the definition of the unresolved scales by means of the cell-agglomeration projector. They proposed instead a Fourier-Spectral projector which could be implemented with a discontinuous Galerkin method. Levasseur *et al.* (2006) and Dahmen *et al.* (2011) implemented the turbulence modeling concept and presented turbulence energy spectra results for turbulent compressible flows.

The stabilization methods proposed in this work are based on the variational multi-scale framework introduced by Hughes (1995) for the scalar convection-diffusion-reaction problem. The method splits the unknowns of the problem into a coarse-scale that belongs to the finite element space and a subgrid scale or subscale, which is the remainder. The original problem is subdivided into two separated problems, one for the finite element scale, and another for the subscales. To avoid increasing the number of degrees of freedom of the problem, an approximation over the subscales is done in terms of the resolved scales. In order to properly do this approximation, we propose to study the behavior of the compressible problem from the perspective of a Fourier analysis, instead of the previous approximations (Rispoli and Saavedra, 2006; Marras *et al.*, 2013). Hence, we aim to give a systematic way to design the approximation over the subscales, that is, to define the matrix of algorithmic parameters for the compressible case.

Downloaded by Kungliga Tekniska Högskolan At 05:21 18 May 2016 (PT)

The main idea of the variational multi-scale stabilization formulation is to include the effect of the unresolved scales in order to stabilize the finite element equations. The variational multi-scale stabilized finite element formulation was introduced to solve the compressible Navier-Stokes equations by Rispoli and Saavedra (2006). They extended satisfactorily the formulation previously done for the incompressible Navier-Stokes equations by Rispoli *et al.* (2007). In that work, they demonstrated the matrix of algorithmic parameters definition for a one-dimensional advective-diffusive-reactive problem on quadratic elements. The contribution of the subscales into the resolved scales was done by integrating by parts the finite element scale equation. More recently, Marras *et al.* (2013) applied the variational multi-scale method in order to stabilize the Euler equations, and demonstrated convergence of the method in a widespread range of stratified flows. They implemented a linear explicit Euler time integration scheme. Even though the variational multi-scale formulation of the compressible problem has already been worked by the last mentioned authors, we incorporate some particular features that we have applied in other flow problems (e.g. Codina *et al.*, 2007; Baiges and Codina, 2010). Since there are different ways to define the subscales, three different approaches are solved in this work. The first possibility is the definition of the space of the subscales, which can be either the space of finite element residuals, or the space orthogonal to the finite element space (Codina, 2000, 2011). The second possibility is the inclusion of the transient term of the subscales equation (Codina *et al.*, 2007). The third possibility is the inclusion of the subscales in all the non-linear terms of the problem (Codina, 2001). In addition to these definitions, we take into account the volumetric part of the convective term in the compressible non-linear operator adjoint, which has not been proposed before in the stabilized formulations.

Furthermore, at supersonic regime some localized instabilities may arise from sharp gradients in the solution, which are inherent to the physics of the problem. Hence, the stabilized formulation requires to be complemented with a local shock capturing term, in order to yield stability and convergence in the entire domain. The first approach was the residual-based shock capturing techniques that controls oscillations in a non-linear fashion depending on the solution. This type of shock capturing operator was introduced by Hughes and Mallet (1986) and later by Le Beau and Tezduyar (1991) into the SUPG compressible flow formulation. Mittal and Tezduyar (1998), Mittal (1998), Hughes *et al.* (2010), and Kotteda and Mittal (2014) continued developing shock capturing stabilized formulations. In contrast with previous formulations (e.g. Tezduyar and Senga, 2006; Sevilla *et al.*, 2013; Woopen *et al.*, 2014) we aim to introduce the numerical diffusion in a "physical manner" for the compressible problem. That is, we modify the diffusion of the momentum and energy equations, but avoid introducing artificial diffusion into the mass equation. In this topic, we also propose to use the orthogonal projection onto the finite element space of the gradient of the unknown, instead of the common residual definition. Because the subgrid stabilization method works in the streamline direction, we implement an anisotropic shock capturing method that keeps the diffusion unaltered in the direction of the streamlines, but modifies the crosswind diffusion. The scope of this proposed shock capturing technique is evaluated with some numerical examples.

Solving the finite element system of equations in an implicit fashion can be computationally very expensive. Our various applications of the compressible formulation, some of which require the solution of small spatial and temporal scales

Downloaded by Kungliga Tekniska Högskolan At 05:21 18 May 2016 (PT)

(such as turbulent flows and aeroacoustics problems), have prompted us to implement explicit time integration schemes, which are reasonably in line with these needs. Therefore, we use an explicit time integration scheme in order to integrate the temporal derivatives, more precisely, we implement the family of explicit Runge-Kutta (RK) methods. Moreover, we calculate the time integration method for the temporal derivative of the dynamic subscales exploiting the explicit scheme adopted.

We perform numerical tests of the formulations presented. The first section of tests corresponds to the study of the formulations in the subsonic range, where there is no need for local stabilization and it is possible to compare the global stabilized formulations. We implement the three-dimensional lid-driven cavity and the flow past a cylinder problems, both in the subsonic range, and benchmark our solutions to those published by other authors. We use the cylinder results obtained with linear triangular elements to compare the convergence of the proposed methods. As another type of test, we make a comparison between the shock capturing methods (proposed in this paper) using the supersonic reflected shock problem. Finally, we present the solution for the compressible viscid supersonic flow past a cylinder including the global and local stabilization methods. This example closes the evaluation of the formulation.

This paper is organized as follows. In Section 2 we present the compressible Navier-Stokes problem. Section 3 contains the numerical approximation using the variational multi-scale finite element formulation of the compressible Navier-Stokes equations. We also present the demonstration of the matrix of stabilization parameters, and the distinct approaches to solve the subscales equation. The shock capturing methods and the explicit time integration scheme are also discussed in Section 3. In Section 4 the numerical examples are presented, and the proposed stabilization is discussed. Finally, in Section 5 conclusions are stated.

2. The compressible Navier-Stokes problem

2.1 Initial and boundary value problem

The problem we consider consists in the Navier-Stokes equations posed in a time interval $(0,T)$ and in a domain $\Omega \subset \mathbb{R}^d$, being d the number of space dimensions ($d=2$ or 3). Let $t \in (0,T)$ be a given time instant in the temporal domain, and $\boldsymbol{x} \in \Omega$ a given point in the spatial domain. Let Γ be the boundary of the domain Ω, and $\boldsymbol{n}$ the geometric unit outward normal vector on Γ. We split Γ into two sets: the Dirichlet boundary denoted as Γ_g, and the Neumman boundary denoted as Γ_n. Considering a compressible, Newtonian and viscous fluid, the governing equations are the conservation of mass, momentum, and energy written in conservation form:

$$\frac{\partial \rho}{\partial t} + \frac{\partial}{\partial x_i}(\rho u_i) = 0, \tag{1}$$

$$\frac{\partial}{\partial t}(\rho u_i) + \frac{\partial}{\partial x_j}\left(\rho u_j u_i + p\delta_{ij} - \tau_{ji}\right) = \rho f_i, \tag{2}$$

$$\frac{\partial}{\partial t}\left(\rho\left(e + \frac{1}{2}u_i u_i\right)\right) + \frac{\partial}{\partial x_j}\left(\rho u_j\left(\mathrm{h} + \frac{1}{2}u_i u_i\right) - u_i \tau_{ij} + q_j\right) = \rho f_i u_i + \rho r, \tag{3}$$

Downloaded by Kungliga Tekniska Högskolan At 05:21 18 May 2016 (PT)

together with appropriate boundary and initial conditions. The usual summation convention is implied in the equations presented before, with indices running from 1 to d. In these equations ρ is the density, p the pressure, $\boldsymbol{u}$ the velocity, $\boldsymbol{\tau}$ the viscous stress tensor, $\boldsymbol{f}$ a body force vector, e the internal energy, h the enthalpy, $\boldsymbol{q}$ the heat flux vector, r a heat source/sink term and $\boldsymbol{I}=[\delta_{ij}]$ is the identity or Kronecker tensor. Supplementary constitutive relations are considered in order to close the problem. For the viscous part of the stress tensor we use the relation:

$$\tau_{ij}(\boldsymbol{u}) = \mu\left(\frac{\partial u_i}{\partial x_j}+\frac{\partial u_j}{\partial x_i}\right)-\frac{2\mu}{3}\left(\frac{\partial u_l}{\partial x_l}\right)\delta_{ij}, \tag{4}$$

where μ is the viscosity. For the heat flux vector we use Fourier's law:

$$q_i(\theta) = -\lambda\frac{\partial \theta}{\partial x_i}, \tag{5}$$

where λ is the thermal conductivity and θ is the temperature of the fluid. The caloric equation $e = c_v(\theta)\theta$ and the perfect gas state equation $p = \rho R\theta$ are used to calculate the pressure and the acoustic speed c. In these relations the specific heat at constant volume $c_v(\theta)$ and the specific heat at constant pressure $c_p(\theta)$ are thermodynamic properties of the fluid. We also define $\gamma = c_p/c_v$ for the ratio between the specific heats, and $R = c_p - c_v$ for the specific gas constant.

Hereafter, let us denote the transpose operation by the superscript $\top$. We write the conservation Equations (1)-(3) in system form introducing the vector of conservative variables $\boldsymbol{U} = [\rho, \boldsymbol{m}, e_{\text{tot}}]^\top$, with density, momentum $\boldsymbol{m} = \rho\boldsymbol{u}$ and total energy $e_{\text{tot}} = \rho(e + \boldsymbol{u}\cdot\boldsymbol{u}/2)$ as its components. The system form of the compressible Navier-Stokes equations written in conservation variables is:

$$\partial_t \boldsymbol{U} + \partial_j \boldsymbol{F}_j(\boldsymbol{U}) + \partial_j \mathbf{G}_j(\boldsymbol{U}) - \boldsymbol{S}(\boldsymbol{U}) = 0 \quad \text{in} \quad \Omega \subset \mathbb{R}^d, t \in (0, T), \tag{6}$$

together with appropriate boundary and initial conditions. Here ∂_t and ∂_j are short notations that indicate the Eulerian time derivative and $\partial/\partial x_j$, respectively. The convective flux in the jth-direction $\boldsymbol{F}_j$ and the diffusive flux in the jth-direction $\boldsymbol{G}_j$ are defined as:

$$\boldsymbol{F}_j(\boldsymbol{U}) = \begin{bmatrix} \rho u_j \\ \rho u_j u_1 + p\delta_{1j} \\ \rho u_j u_2 + p\delta_{2j} \\ \rho u_j u_3 + p\delta_{3j} \\ u_j(e_{\text{tot}} + p) \end{bmatrix}, \boldsymbol{G}_j(\boldsymbol{U}) = \begin{bmatrix} 0 \\ -\tau_{j1} \\ -\tau_{j2} \\ -\tau_{j3} \\ -u_i\tau_{ij} + q_j \end{bmatrix}.$$

The divergence of these fluxes is written in a more convenient manner as $\partial_j \boldsymbol{F}_j(\boldsymbol{U}) = \boldsymbol{A}_j(\boldsymbol{U})\partial_j \boldsymbol{U}$ and $\partial_j \boldsymbol{G}_j(\boldsymbol{U}) = -\partial_k(\boldsymbol{K}_{kj}(\boldsymbol{U})\partial_j \boldsymbol{U})$, with the definition of the Euler Jacobian matrix $\boldsymbol{A}_j(\boldsymbol{U}) = \partial \boldsymbol{F}_j(\boldsymbol{U})/\partial \boldsymbol{U}$, and the diffusivity matrix $\boldsymbol{K}(\boldsymbol{U}) = [\boldsymbol{K}_{kj}(\boldsymbol{U})]$. As a remark, both the Euler Jacobian and the diffusivity matrices depend on the variables of unknowns through the constitutive relations of the fluid. The last term, the vector of *sources*

$\boldsymbol{S}(\boldsymbol{U}) = [0,\ \rho\boldsymbol{f},\ \rho\boldsymbol{f}\cdot\boldsymbol{u}+\rho r]^{\top}$, contains the right hand side terms of Equations (1)-(3). We can linearize this term by introducing a reactive matrix:

$$\boldsymbol{S} = \begin{bmatrix} 0 & 0 & 0 \\ \boldsymbol{f} & 0 & 0 \\ r & \boldsymbol{f}^{\top} & 0 \end{bmatrix}, \tag{7}$$

that multiplies the vector of unknowns $\boldsymbol{S}(\boldsymbol{U}) = \boldsymbol{S}\boldsymbol{U}$. The non-linear operator:

$$\mathcal{L}\left(\check{\boldsymbol{U}};\boldsymbol{U}\right) = \mathbf{A}_j\left(\check{\boldsymbol{U}}\right)\partial_j\boldsymbol{U} - \partial_k\left(\boldsymbol{K}_{kj}\left(\check{\boldsymbol{U}}\right)\partial_j\boldsymbol{U}\right) - \boldsymbol{S}\boldsymbol{U}, \tag{8}$$

includes the previous definitions for the convective, diffusive, and reactive terms. The non-linearity in the first argument of the operator arises from the dependency of the Euler Jacobian and diffusivity matrices on the unknowns. However, the operator is linear in the second argument.

Equation (6) may be now written using the non-linear operator as:

$$\partial_t\boldsymbol{U} + \mathcal{L}(\boldsymbol{U};\boldsymbol{U}) = \boldsymbol{0} \qquad \text{in}\ \Omega \subset \mathbb{R}^d, t \in (0,T). \tag{9}$$

The compressible Navier-Stokes problem is a non-linear initial and boundary value problem of hyperbolic type, subject to appropriate definitions for the boundary and initial conditions, which can be written in vector form as:

$$\boldsymbol{F}_j n_j = \boldsymbol{h} \qquad \text{on}\ \Gamma_n, t \in (0,T), \tag{10}$$

$$\mathcal{U}(\boldsymbol{U}) = \boldsymbol{U}_g \qquad \text{on}\ \Gamma_g, t \in (0,T), \tag{11}$$

$$\boldsymbol{U} = \boldsymbol{U}_0(\boldsymbol{x}) \qquad \text{in}\ \Omega, t = 0. \tag{12}$$

On the one hand, Neumann boundary conditions $\boldsymbol{h}$ are convective fluxes. On the other hand, the Dirichlet boundary operator $\mathcal{U}(\cdot)$ is used to impose the Dirichlet boundary conditions $\boldsymbol{U}_g$. Due to the hyperbolic and compressible nature of the problem, Dirichlet boundary conditions must be imposed in the inlet part of the boundary $\Gamma_{\text{in}} = \{\boldsymbol{x} \in \Gamma | (\boldsymbol{u}\cdot\boldsymbol{n})(\boldsymbol{x}) < 0\}$. For the sake of simplicity we have grouped Neumann conditions on Γ_n and Dirichlet conditions on Γ_g, but mixed types of conditions could be applied to different variables (momentum and total energy) on the same part of the boundary.

The non-dimensional Mach number $M = |\boldsymbol{u}|/c$ is used to calculate the compressibility regime. It can range from subsonic ($M < 0.8$), transonic ($0.8 < M < 1.2$), supersonic ($M > 1.2$), and hypersonic flow ($M \gg 1$). Here we focus our attention to the subsonic, transonic, and supersonic regimes. All conservative variables are imposed at the inflow part of the Dirichlet boundary, regardless the compressibility regime. For the supersonic case, no Dirichlet conditions need to be imposed at the outflow, defined as $\Gamma_{\text{out}} = \{\boldsymbol{x} \in \Gamma | (\boldsymbol{u}\cdot\boldsymbol{n})(\boldsymbol{x}) > 0\}$. In the case of subsonic flow, only density is imposed at the outflow boundary Γ_{out}. Solid boundaries can be represented as a slip condition $\boldsymbol{u}\cdot\boldsymbol{n} = 0$, as a no-slip condition $\boldsymbol{u} = 0$, or as an isothermal wall $e_{\text{tot}} = \rho c_v \theta$. In addition, initial conditions for the conservative variables must be defined at $t = 0$, which are of the form $\boldsymbol{U} = \boldsymbol{U}_0(\boldsymbol{x})$, with $\boldsymbol{U}_0(\boldsymbol{x})$ functions defined on the whole domain Ω. We will explicitly indicate in our examples how the initial and boundary conditions are prescribed.

Downloaded by Kungliga Tekniska Högskolan At 05:21 18 May 2016 (PT)

Downloaded by Kungliga Tekniska Högskolan At 05:21 18 May 2016 (PT)

2.2 The variational problem

Let us introduce some notation in order to write the variational form of the problem. Let $L^2(\Omega)$ be the space of square integrable functions in the domain Ω. We use the symbol $\langle .,. \rangle$ to denote the integral of the product of two functions, including the dual pairing, assuming it is well defined. The L^2 inner product in Ω is denoted by $(\cdot,\cdot)$.

Let $\mathcal{W}$ be an appropriate test functions space. The weak form of the problem is obtained by testing (9) against an arbitrary test function V. The weak form can be written as: find U belonging to the space of unknowns, such that:

$$(V, \partial_t U) + \langle V, \mathcal{L}(U; U) \rangle = 0 \quad \forall V \in \mathcal{W}, \tag{13}$$

together with appropriate sets of boundary and initial conditions.

3. Numerical approximation

3.1 The Galerkin finite element discretization

The FEM approximation of the continuous variational problem (13) can be done with the standard Galerkin method. Let us consider the finite element partition $\mathcal{T}_h = \{K\}$ of the domain Ω. The diameter of the element partition is denoted by h. We define the test functions space $\mathcal{W}_h \subset \mathcal{W}$ as continuous picewise polynomial in space. The Galerkin FEM problem consists of finding a finite element solution U_h belonging to the trial space, such that:

$$(V_h, \partial_t U_h) + \langle V_h, \mathcal{L}(U_h; U_h) \rangle = 0 \forall V_h \in \mathcal{W}_h, \tag{14}$$

together with the appropriate initial and boundary conditions of the problem. When the Galerkin method is used to solve this hyperbolic problem, which possesses non-symmetric operators, an unstable behavior of the solution might appear when the convection is dominant, and due to the incompatibility of the interpolation of the different variables.

3.2 The space discrete variational multi-scale stabilized finite element formulation

We present a stabilized formulation for the compressible Navier-Stokes equations based on the variational multi-scale approach introduced by Hughes (1995). The basic idea is to approximate the effect of the components of the solution of the continuous problem that cannot be solved by the finite element mesh. It consists on the decomposition of the unknown $U = U_h + \widetilde{U}$, into a coarse-scale $U_h \in \mathcal{W}_h$ that belongs to the finite element space and a subgrid scale or subscale $\widetilde{U} \in \widetilde{\mathcal{W}}$, which is the remainder. The spaces $\mathcal{W}_h$ and $\widetilde{\mathcal{W}}$ are such that $\mathcal{W} = \mathcal{W}_h \oplus \widetilde{\mathcal{W}}$. Hence, consistently $V = V_h + \widetilde{V}$, where $V_h \in \mathcal{W}_h$ and $\widetilde{V} \in \widetilde{\mathcal{W}}$. The variational formulation (13) can now be split into two equivalent subproblems:

$$(V_h, \partial_t U) + \langle V_h, \mathcal{L}(U; U) \rangle = 0 \quad \forall V_h \in \mathcal{W}_h, \tag{15}$$

$$\left(\widetilde{V}, \partial_t U\right) + \left\langle \widetilde{V}, \mathcal{L}(U; U) \right\rangle = 0 \quad \forall \widetilde{V} \in \widetilde{\mathcal{W}}. \tag{16}$$

The objective is to approximate the subscales in order to end up with a problem for the finite element scale alone. On the one hand, we integrate by parts Equation (15) and obtain:

$$(V_h, \partial_t U) + \langle V_h, \mathcal{L}(U; U_h) \rangle + \left\langle \mathcal{L}^*(U; V_h), \widetilde{U} \right\rangle = 0 \quad \forall V_h \in \mathcal{W}_h. \tag{17}$$

Here we have introduced the formal adjoint $\mathcal{L}^*(U,)$ of the operator $\mathcal{L}^*(\boldsymbol{U},)$. The adjoint operator is defined as $\langle \boldsymbol{V}, \mathcal{L}(\boldsymbol{U}; \boldsymbol{W})\rangle = \langle \mathcal{L}^*(\boldsymbol{U}; \boldsymbol{V}), \boldsymbol{W}\rangle$, for all $\boldsymbol{U}$, $\boldsymbol{V}$, $\boldsymbol{W} \in \boldsymbol{\mathcal{W}}$. The duality might involve inter-element jump terms when finite element functions are considered. However, these inter-element terms are neglected by supposing that the subscales vanish at the element boundaries. With the above approximation, the outcome for the adjoint of the non-linear operator (8) applied to the test functions vector is:

$$\mathcal{L}^*(\boldsymbol{U}; \boldsymbol{V}_h) = -\partial_j\left(\boldsymbol{A}_j^\top(\boldsymbol{U})\boldsymbol{V}_h\right) - \partial_j\left(\boldsymbol{K}_{kj}^\top(\boldsymbol{U})\partial_k \boldsymbol{V}_h\right) - \boldsymbol{S}^\top \boldsymbol{V}_h. \tag{18}$$

It is important to remark the contribution of the derivative of the Euler Jacobian matrix in the first term on the right hand side. In this work we linearize the derivatives of the first and second terms on the right hand side of the previous expression, respectively as:

$$\frac{\partial}{\partial x_j}\left(\boldsymbol{A}_j^\top(\boldsymbol{U})\boldsymbol{V}_h\right) \approx \boldsymbol{A}_j^\top(\boldsymbol{U})\frac{\partial \boldsymbol{V}_h}{\partial x_j} + \frac{\partial \boldsymbol{A}_j^\top(\boldsymbol{U})}{\partial \boldsymbol{U}}\frac{\partial \boldsymbol{U}_h}{\partial x_j}\boldsymbol{V}_h, \tag{19}$$

$$\frac{\partial}{\partial x_j}\left(\boldsymbol{K}_{kj}^\top(\boldsymbol{U})\frac{\partial \boldsymbol{V}_h}{\partial x_k}\right) \approx \boldsymbol{K}_{kj}^\top(\boldsymbol{U})\frac{\partial^2 \boldsymbol{V}_h}{\partial x_j \partial x_k} + \frac{\partial \boldsymbol{K}_{kj}^\top(\boldsymbol{U})}{\partial \boldsymbol{U}}\frac{\partial \boldsymbol{U}_h}{\partial x_j}\frac{\partial \boldsymbol{V}_h}{\partial x_k}. \tag{20}$$

We complete the formulation for the finite element scale equation by integrating by parts the diffusive term of the non-linear operator applied to the finite element unknowns. Since the normal component of the diffusive flux must be continuous across inter-element boundaries:

$$\sum_K \left(\boldsymbol{V}_h,\ n_k \boldsymbol{K}_{kj}(\boldsymbol{U})\partial_j \boldsymbol{U}\right)_{\partial K} = 0 \quad \forall \boldsymbol{V}_h \in \mathcal{W}_h, \tag{21}$$

the equation for the finite element scale results in:

$$\begin{aligned}&\left(\boldsymbol{V}_h,\ \partial_t \boldsymbol{U}_h\right) + \left(\boldsymbol{V}_h,\ \partial_t \widetilde{\boldsymbol{U}}\right) + \left(\boldsymbol{V}_h,\ \boldsymbol{A}_j(\boldsymbol{U})\partial_t \boldsymbol{U}_h\right) + \left(\partial_k \boldsymbol{V}_h,\ \boldsymbol{K}_{kj}(\boldsymbol{U})\partial_j \boldsymbol{U}_h\right)\\ &-\left(\boldsymbol{V}_h,\ \boldsymbol{S}\boldsymbol{U}_h\right) + \sum_K \left\langle \mathcal{L}^*(\boldsymbol{U};\ \boldsymbol{V}_h),\ \widetilde{\boldsymbol{U}}\right\rangle_K = 0 \quad \forall \boldsymbol{V}_h \in \boldsymbol{\mathcal{W}}_h.\end{aligned} \tag{22}$$

In the previous equation, $\langle \cdot, \cdot \rangle_K$ denotes the L^2 inner product over the element K.

On the other hand, if $\widetilde{\boldsymbol{P}}$ denotes the L^2-projection onto the space of subscales, the equation for the subgrid scale can be formally written as:

$$\widetilde{\boldsymbol{P}}\left[\partial_t \widetilde{\boldsymbol{U}} + \mathcal{L}\left(\boldsymbol{U}; \widetilde{\boldsymbol{U}}\right)\right] = \widetilde{\boldsymbol{P}}[\boldsymbol{R}(\boldsymbol{U}; \boldsymbol{U}_h)], \tag{23}$$

where $\boldsymbol{R}(\cdot, \cdot) = (R_\rho(\cdot, \cdot), \boldsymbol{R}_{\boldsymbol{m}}(\cdot, \cdot), R_{e_{\text{tot}}}(\cdot, \cdot))^\top$ stands for the residual vector, which is composed by the equations residuals, and is formally defined as:

$$\boldsymbol{R}\left(\check{\boldsymbol{U}}; \boldsymbol{U}\right) = -\partial_t \boldsymbol{U} - \mathcal{L}\left(\check{\boldsymbol{U}}; \boldsymbol{U}\right). \tag{24}$$

Since the subscales cannot be represented by the finite element mesh, the effect of the non-linear operator applied to the subscales needs to be approximated. For this,

Downloaded by Kungliga Tekniska Högskolan At 05:21 18 May 2016 (PT)

Downloaded by Kungliga Tekniska Högskolan At 05:21 18 May 2016 (PT)

we adopt a diagonal matrix of stabilization parameters that depends on the unknowns $\boldsymbol{\tau}(\boldsymbol{U})$, such that an approximation of the non-linear operator applied to the subscales is made in each element:

$$\boldsymbol{\mathcal{L}}\left(\boldsymbol{U};\widetilde{\boldsymbol{U}}\right)\approx\boldsymbol{\tau}^{-1}(\boldsymbol{U})\widetilde{\boldsymbol{U}}. \tag{25}$$

The way to construct this approximation is explained further below. Hence, for an adequate definition of the projection onto the subscales space, the subscales equation is:

$$\widetilde{\boldsymbol{P}}\left[\partial_t\widetilde{\boldsymbol{U}}+\boldsymbol{\tau}^{-1}(\boldsymbol{U})\widetilde{\boldsymbol{U}}\right]=\widetilde{\boldsymbol{P}}\left[\boldsymbol{R}(\boldsymbol{U};\boldsymbol{U}_h)\right]. \tag{26}$$

The previous equation is a non-linear ordinary differential equation, which must be solved at the integration points. There are different approximations in order to calculate $\widetilde{\boldsymbol{U}}$ from this equation.

Here we use two possibilities to construct the space where the subscales belong. The first and the most common choice is to take it equal to the space of the finite element residuals. That is, to define the projection onto the subscales space as the identity $\widetilde{\boldsymbol{P}}=\boldsymbol{I}$ onto the space of finite element residuals. The second possibility is the so-called orthogonal subscales method, which defines the subscales orthogonal to the finite element space $\boldsymbol{W}=\boldsymbol{W}_h^{\perp}$. In this case, the projection is defined to be the orthogonal projection onto the finite element space $\widetilde{\boldsymbol{P}}=\boldsymbol{P}_h^{\perp}=\boldsymbol{I}-\boldsymbol{P}_h$, being $\boldsymbol{P}_h$ the L^2-projection onto the finite element space.

Apart from the construction of the spaces where the subscales belong, we call the subscales dynamic if the temporal derivative of subscales is taken into account. Instead, if the temporal derivative of the subscales is neglected we call them quasi-static subscales. Another possibility is to neglect the subscales effect in all the non-linear terms, whereas, if we take it into account we call them non-linear subscales.

3.3 The matrix $\boldsymbol{\tau}$ of stabilization parameters

The key point in the design of the stabilized formulation is the construction of the matrix $\boldsymbol{\tau}$. In order to do this we study the behavior of the problem from the perspective of a Fourier analysis. This strategy was introduced in some other formulations (Codina *et al.*, 2008; Codina, 2009), and we apply it to the compressible Navier-Stokes problem. We basically want to bound the effect of the non-linear operator, and approximate it with matrix $\boldsymbol{\tau}^{-1}$. First, let us consider the following Fourier transform denoted by $\widehat{\cdot}$, and defined on each element K:

$$\widehat{g}(\boldsymbol{k}):=\int_K e^{-i\frac{\boldsymbol{k}\cdot\boldsymbol{x}}{h}}g(\boldsymbol{x})d\Omega_x, \tag{27}$$

where $i=\sqrt{-1}$. The wave number $\boldsymbol{k}$ is defined as $\boldsymbol{k}=(k_1,...,k_d)$, and h as the diameter of K. If n_j is the jth component of the normal exterior to K, it can be checked that:

$$\widehat{\frac{\partial g}{\partial x_j}}(\boldsymbol{k})=\int_{\partial K}n_j\mathrm{e}^{-\mathrm{i}\frac{\boldsymbol{k}\cdot\boldsymbol{x}}{h}}g(\boldsymbol{x})d\Gamma_x+\mathrm{i}\frac{k_j}{h}\widehat{g}(\boldsymbol{k}). \tag{28}$$

The basic heuristic assumption is that $\widetilde{\boldsymbol{U}}$ is highly fluctuating, and therefore only contains high wave numbers:

$$\widehat{\frac{\partial\widetilde{\mathbf{U}}}{\partial x_j}}(\boldsymbol{k})\approx\mathrm{i}\frac{k_j}{h}\widehat{\widetilde{\boldsymbol{U}}}(\boldsymbol{k}). \tag{29}$$

Downloaded by Kungliga Tekniska Högskolan At 05:21 18 May 2016 (PT)

As a consequence, we may assume that values of $\widetilde{\boldsymbol{U}}$ on ∂K can be neglected to approximate $\widetilde{\boldsymbol{U}}$ in the interior of K. In addition, we can linearize $\boldsymbol{\mathcal{L}}(\boldsymbol{U}, \widetilde{\boldsymbol{U}}) \approx \boldsymbol{\mathcal{L}}\widetilde{\boldsymbol{U}}$ by considering $\boldsymbol{U}$ as given and constant in the non-linear convective and diffusive matrices of (8). Taking into account the above considerations, we calculate the Fourier transform of $\boldsymbol{\mathcal{L}}\widetilde{\boldsymbol{U}}$ as:

$$\widehat{\boldsymbol{\mathcal{L}}}(\boldsymbol{k})\widehat{\widetilde{\boldsymbol{U}}}(\boldsymbol{k}) = \mathrm{i}\frac{k_j}{h}\boldsymbol{A}_j\widehat{\widetilde{\boldsymbol{U}}}(\boldsymbol{k}) + \frac{k_k k_j}{h^2}\boldsymbol{K}_{kj}\widehat{\widetilde{\boldsymbol{U}}}(\boldsymbol{k}) - \boldsymbol{S}\widehat{\widetilde{\boldsymbol{U}}}(\boldsymbol{k}). \tag{30}$$

The proper scaling of the problem is crucial to discuss the approximation of matrix $\boldsymbol{\tau}^{-1}$. Let $\boldsymbol{U}$, $\boldsymbol{V}$ be elements in the domain of $\boldsymbol{\mathcal{L}}\mathbf{U}$ and $\boldsymbol{F}$, $\boldsymbol{G}$ elements in its range. Suppose that $\boldsymbol{\mathcal{L}}\boldsymbol{U} = \boldsymbol{F}$ is written in such a way that $\boldsymbol{F}^{\mathrm{T}}\boldsymbol{U}$ is dimensionally well defined. Let also the $\boldsymbol{M}-$norm of $\boldsymbol{F}$ be defined as $|\boldsymbol{F}|^2_{\mathbf{M}} := \boldsymbol{F}^\top\boldsymbol{M}\boldsymbol{F}$, the $\boldsymbol{M}^{-1}-$norm of $\boldsymbol{U}$ as $|\boldsymbol{U}|^2_{M^{-1}} := \boldsymbol{U}^\top\boldsymbol{M}^{-1}\boldsymbol{U}$, and $\|\boldsymbol{F}\|^2_{L^2_{\mathbf{M}}(K)} := \int_K |\boldsymbol{F}|^2_{\boldsymbol{M}}$. In order to compare in a consistent manner the previously defined norms, we introduce the scaling matrix $\boldsymbol{M}$ that makes dimensionally correct the products:

$$\boldsymbol{F}^\top\boldsymbol{M}\boldsymbol{G} \quad \text{and} \quad \boldsymbol{U}^\top\boldsymbol{M}^{-1}\boldsymbol{V}. \tag{31}$$

We propose that the stabilization matrix $\boldsymbol{\tau}^{-1}$ must be such that $\|\boldsymbol{\mathcal{L}}\|_{L^2_M(K)} \leqslant \|\boldsymbol{\tau}^{-1}\|_{L^2_{\mathbf{M}}(K)}$. In order to devise a way to satisfy it, let us note that:

$$\begin{aligned}
\|\boldsymbol{\mathcal{L}}\widetilde{\boldsymbol{U}}\|_{L^2_M(K)} &= \int_K \left|\boldsymbol{\mathcal{L}}\widetilde{\boldsymbol{U}}\right|^2_M dx \approx \int_{\mathbb{R}^d} \left|\widehat{\boldsymbol{\mathcal{L}}}(k)\widehat{\widetilde{\boldsymbol{U}}}(k)\right|^2_M d\boldsymbol{k} \\
&\leqslant \int_{\mathbb{R}^d} \left|\widehat{\boldsymbol{\mathcal{L}}}(k)\right|^2_M \left|\widehat{\widetilde{\boldsymbol{U}}}(k)\right|^2_{M^{-1}} d\boldsymbol{k} \\
&= \left|\widehat{\boldsymbol{\mathcal{L}}}\left(k^0\right)\right|^2_M \int_{\mathbb{R}^d} \left|\widehat{\widetilde{\boldsymbol{U}}}(k)\right|^2_{M^{-1}} d\boldsymbol{k} \approx \left|\widehat{\boldsymbol{\mathcal{L}}}\left(\boldsymbol{k}^0\right)\right|^2_M \|\widetilde{\boldsymbol{U}}\|^2_{L^2_{M^{-1}}(K)},
\end{aligned} \tag{32}$$

where the first approximation comes from the fact that boundary values of $\widetilde{\boldsymbol{U}}$ have been discarded, and $\boldsymbol{k}^0$ is a wave number whose existence follows from the mean value theorem. From the previous development we have that

$$\|\boldsymbol{\mathcal{L}}\|_{L^2_M(K)} \leqslant \left|\widehat{\boldsymbol{\mathcal{L}}}\left(\boldsymbol{k}^0\right)\right|^2_M. \tag{33}$$

Our proposal is to choose $\boldsymbol{\tau}$ diagonal and such that $|\widehat{\boldsymbol{\mathcal{L}}}(\mathbf{k}^0)|^2_M = |\boldsymbol{\tau}^{-1}|^2_M$, with the components of $\boldsymbol{k}^0$ understood as algorithmic constants. From (32) we can figure out the following way to achieve this approximation:

$$\left|\widehat{\boldsymbol{\mathcal{L}}}\left(\boldsymbol{k}^0\right)\right|^2_M = \sup_{\widehat{\widetilde{\boldsymbol{U}}}} \frac{\left(\widehat{\widetilde{\boldsymbol{U}}}, \widehat{\boldsymbol{\mathcal{L}}}\left(\boldsymbol{k}^0\right)^* \boldsymbol{M}\widehat{\boldsymbol{\mathcal{L}}}\left(\boldsymbol{k}^0\right)\widehat{\widetilde{\boldsymbol{U}}}\right)}{\left(\widehat{\widetilde{\boldsymbol{U}}}, \boldsymbol{M}^{-1}\widehat{\widetilde{\boldsymbol{U}}}\right)}, \tag{34}$$

with $\widehat{\widetilde{\boldsymbol{U}}}^* \widehat{\boldsymbol{\mathcal{L}}}(\boldsymbol{k}^0)^* \boldsymbol{M}\widehat{\boldsymbol{\mathcal{L}}}(\boldsymbol{k}^0)\widehat{\widetilde{\boldsymbol{U}}} \in \mathbb{R}^+$ but $\widehat{\widetilde{\boldsymbol{U}}}^*$, $\widehat{\boldsymbol{\mathcal{L}}}(\boldsymbol{k}^0)^*$, $\widehat{\boldsymbol{\mathcal{L}}}(\boldsymbol{k}^0)$, and $\widehat{\widetilde{\boldsymbol{U}}}$, being complex.

Let us denote by $\mathrm{spec}_{M^{-1}}(\boldsymbol{B})$ the spectrum of the generalized eigenvalue problem $\boldsymbol{B}\boldsymbol{x} = \lambda\boldsymbol{M}^{-1}\boldsymbol{x}$, being λ an eigenvalue, and its spectral radius by $\check{\rho}(\boldsymbol{B})$. Equation (34) is

Downloaded by Kungliga Tekniska Högskolan At 05:21 18 May 2016 (PT)

equivalent to the following eigenvalue problem: if there exists $\widehat{\widetilde{\boldsymbol{U}}}$ such that $(\widehat{\boldsymbol{\mathcal{L}}}(\boldsymbol{k}^0)^{*}\boldsymbol{M}\widehat{\boldsymbol{\mathcal{L}}}(\boldsymbol{k}^0))\widehat{\widetilde{\boldsymbol{U}}} = \lambda \boldsymbol{M}^{-1}\widehat{\widetilde{\boldsymbol{U}}}$, then:

$$\left|\widehat{\boldsymbol{\mathcal{L}}}\left(\boldsymbol{k}^0\right)\right|_M^2 = \max \operatorname{spec}_{M^{-1}}\left(\widehat{\boldsymbol{\mathcal{L}}}\left(\boldsymbol{k}^0\right)^{*}\boldsymbol{M}\widehat{\boldsymbol{\mathcal{L}}}\left(\boldsymbol{k}^0\right)\right). \tag{35}$$

Furthermore, in this work we propose to estimate separately each contribution of the convective, diffusive and reactive terms of (30), since:

$$\left|\widehat{\boldsymbol{\mathcal{L}}}\left(\boldsymbol{k}^0\right)\right|_M^2 \leqslant \left|\widehat{\boldsymbol{\mathcal{L}}}_C\left(\boldsymbol{k}^0\right)\right|_M^2 + \left|\widehat{\boldsymbol{\mathcal{L}}}_D\left(\boldsymbol{k}^0\right)\right|_M^2 + \left|\widehat{\boldsymbol{\mathcal{L}}}_R\left(\boldsymbol{k}^0\right)\right|_M^2, \tag{36}$$

where subindices C, D and R denote the convective, diffusive, and reactive terms, respectively. We aim to analyze the one-dimensional case in the x_1 direction, and thereafter generalize to multiple d dimensions.

3.3.1 Convective term. The solution of the one-dimensional hyperbolic problem:

$$\boldsymbol{\mathcal{L}}_C(\boldsymbol{U}) = \boldsymbol{A}\frac{\partial \boldsymbol{U}}{\partial x_1}, \tag{37}$$

is bounded by the eigenvalues of the Jacobian matrix. The one-dimensional linearized Euler Jacobian matrix:

$$\boldsymbol{A} = \begin{bmatrix} 0 & 1 & 0 \\ (\gamma-3)\frac{u_1^2}{2} & (3-\gamma)u_1 & (\gamma-1) \\ (\gamma-1)u_1^3 - \gamma\frac{u_1 e_{\text{tot}}}{\rho} & \gamma\frac{e_{\text{tot}}}{\rho} - (\gamma-1)\frac{3u_1^2}{2} & \gamma u_1 \end{bmatrix}, \tag{38}$$

can be decomposed as $\boldsymbol{A} = \boldsymbol{T}\boldsymbol{D}\boldsymbol{T}^{-1}$, with the right and left-eigenvectors matrices defined as:

$$\boldsymbol{T} = \begin{bmatrix} 1 & 1 & 1 \\ u_1 - c & u_1 + c & u_1 \\ -\frac{bu_1^2 + 2cbu_1 - 2}{2b} & \frac{bu^2 + 2cbu_1 + 2}{2b} & \frac{u_1^2}{2} \end{bmatrix}, \boldsymbol{T}^{-1} = \begin{bmatrix} \frac{u_1(cbu_1+2)}{4c} & -\frac{cbu_1+1}{2c} & \frac{b}{2} \\ \frac{u_1(cbu_1-2)}{4c} & -\frac{cbu_1-1}{2c} & \frac{b}{2} \\ -\frac{bu_1^2-2}{2} & bu_1 & -b \end{bmatrix}, \tag{39}$$

and $b = (\gamma-1)/c^2$. For convenience, let us denote as diag($\boldsymbol{e}$) the diagonal matrix with vector $\boldsymbol{e}$ on the diagonal. The diagonal matrix of eigenvalues results from the previous decomposition as:

$$\boldsymbol{D} = \operatorname{diag}(u_1 - c, u_1 + c, u_1). \tag{40}$$

The spectrum of $(\widehat{\boldsymbol{\mathcal{L}}}_C(\boldsymbol{k}^0)^{*}\boldsymbol{M}\widehat{\boldsymbol{\mathcal{L}}}_C(\boldsymbol{k}^0))$ can be evaluated without difficulty by transforming (37) into a problem which posses $\boldsymbol{D}$ as convective matrix. This can be achieved with a projector defined as the matrix of left-eigenvectors $\boldsymbol{T}^{-1}$. Thus, the unknowns and force vectors can be transformed into:

$$\boldsymbol{W} = \boldsymbol{T}^{-1}\boldsymbol{U} = \left(\frac{\rho}{2\gamma}, \frac{\rho}{2\gamma}, \frac{(\gamma-1)\rho}{\gamma}\right)^{\top}, \tag{41}$$

$$\boldsymbol{H} = \boldsymbol{T}^{-1}\boldsymbol{F} = \left(\frac{\rho u_1}{2\gamma h}, \frac{\rho u_1}{2\gamma h}, \frac{(\gamma-1)\rho u_1}{\gamma h}\right)^{\top}. \tag{42}$$

Because the derivatives of $\boldsymbol{T}^{-1}$ are null as a result of the linearized Euler Jacobian matrix, we can transform the convective problem:

$$\boldsymbol{\mathcal{L}}'_C(\boldsymbol{U}) = \boldsymbol{T}^{-1}\boldsymbol{\mathcal{L}}_C(\boldsymbol{U}), \tag{43}$$

into the following problem:

$$\boldsymbol{\mathcal{L}}'_C(\boldsymbol{W}) = \boldsymbol{D}\frac{\partial \boldsymbol{W}}{\partial x}. \tag{44}$$

Problem (44) is the so-called Riemman problem, used for physical considerations. At this point $\boldsymbol{\mathcal{L}}'_C(\boldsymbol{W}) = \boldsymbol{H}$ is such that $\boldsymbol{H}^{\top}\boldsymbol{W} = \sum_{i=1}^{3} H_i W_i$ is dimensionally well defined. Let $\boldsymbol{W}$, $\boldsymbol{Y}$ be elements in the domain of $\boldsymbol{\mathcal{L}}'_C$ and $\boldsymbol{H}$, $\boldsymbol{J}$ elements in its range. The scaling matrix defined as the identity matrix $\boldsymbol{M} = \boldsymbol{I}$ makes the product $\boldsymbol{H}^{\top}\boldsymbol{M}\boldsymbol{J}$ correct, because $[\rho^2 u_1^2 h^{-2}] = [\rho^2 u_1^2 h^{-2}] = [\rho^2 u_1^2 h^{-2}] = M^2 L^{-6} T^{-2}$, where $[\,\cdot\,]$ stands for dimensional group, M is mass, L is length, and T is time. The product $\boldsymbol{W}^{\top}\boldsymbol{M}^{-1}\boldsymbol{Y}$ is also consistent, indeed $[\rho^2] = [\rho^2] = [\rho^2] = M^2 L^{-6}$.

The previous development makes it possible to analytically calculate the spectrum of $(\widehat{\boldsymbol{\mathcal{L}}}'_C(\boldsymbol{k})^{*}\boldsymbol{M}\widehat{\boldsymbol{\mathcal{L}}}'_C(\boldsymbol{k}))$ with respect to $\boldsymbol{M}^{-1}$, which is given by:

$$\mathrm{spec}_{M^{-1}}\left(\left(\frac{k_1^0}{h}\right)^2 \boldsymbol{D}^{\top}\boldsymbol{M}\boldsymbol{D}\right) = \left\{\left(\frac{k_1^0(u_1+c)}{h}\right)^2, \left(\frac{k_1^0 u_1}{h}\right)^2, \left(\frac{k_1^0(u_1-c)}{h}\right)^2\right\}. \tag{45}$$

Therefore, the spectral radius is given by:

$$\check{\rho}\left(\left(\frac{k_1^0}{h}\right)^2 \boldsymbol{D}^{T}\boldsymbol{M}\boldsymbol{D}\right) = \left(\frac{k_1^0(u_1+c)}{h}\right)^2. \tag{46}$$

If we take the simple diagonal expression for the transformed matrix of stabilization parameters $(\boldsymbol{\tau}')^{-1} = \mathrm{diag}\left((\tau'_{\rho})^{-1}, (\tau'_{m})^{-1}, \left(\tau'_{e_{\mathrm{tot}}}\right)^{-1}\right)$, the spectrum is:

$$\mathrm{spec}_{M^{-1}}\left((\boldsymbol{\tau}')^{-1}\boldsymbol{M}(\boldsymbol{\tau}')^{-1}\right) = \left\{\left(\frac{1}{\tau'_{\rho}}\right)^2, \left(\frac{1}{\tau'_{m}}\right)^2, \left(\frac{1}{\tau'_{e_{\mathrm{tot}}}}\right)^2\right\}. \tag{47}$$

Our proposal is to equate the spectral radius of both problems:

$$\check{\rho}\left((\boldsymbol{\tau}')^{-1}\boldsymbol{M}(\boldsymbol{\tau}')^{-1}\right) = \check{\rho}\left(\left(\frac{k_1^0}{h}\right)^2 \boldsymbol{D}^{T}\boldsymbol{M}\boldsymbol{D}\right). \tag{48}$$

Downloaded by Kungliga Tekniska Högskolan At 05:21 18 May 2016 (PT)

We can fulfill condition (48) by making each eigenvalue of (47) be equal to (46). As a result, the stabilization matrix after retrieving the transformation $\boldsymbol{\tau}^{-1} = \boldsymbol{T}(\boldsymbol{\tau}')^{-1}\boldsymbol{T}^{-1}$ is defined for the one-dimensional convective case as:

$$\boldsymbol{\tau}^{-1} = \begin{bmatrix} \tau_\rho^{-1} & 0 & 0 \\ 0 & \tau_m^{-1} & 0 \\ 0 & 0 & \tau_{e_{\text{tot}}}^{-1} \end{bmatrix}, \text{with, } \tau_\rho^{-1} = \tau_m^{-1} = \tau_{e_{\text{tot}}}^{-1} = \frac{k_1^0(u_1 + c)}{h}. \tag{49}$$

3.3.2 Diffusive term. Furthermore, we also account for the contribution of the one-dimensional diffusive term:

$$\boldsymbol{\mathcal{L}}_D(\boldsymbol{U}) = \frac{\partial}{\partial x_1}\left(\boldsymbol{K}\frac{\partial \boldsymbol{U}}{\partial x_1}\right), \tag{50}$$

by decomposing the one-dimensional linearized diffusivity matrix:

$$\boldsymbol{K} = \begin{bmatrix} 0 & 0 & 0 \\ -\frac{4\nu u_1}{3} & \frac{4\nu}{3} & 0 \\ -\frac{4\nu u_1^2}{3} - \frac{\alpha e_{\text{tot}}}{\rho} + \alpha u_1^2 & \frac{4\nu u_1}{3} - \alpha u_1 & \alpha \end{bmatrix}, \tag{51}$$

into $\boldsymbol{K} = \boldsymbol{T}\boldsymbol{D}\boldsymbol{T}^{-1}$, with:

$$\boldsymbol{T} = \begin{bmatrix} 0 & 0 & 1 \\ 1 & 0 & u_1 \\ u_1 & 1 & \frac{e_{\text{tot}}}{\rho} \end{bmatrix}, \boldsymbol{D} = \begin{bmatrix} \frac{4\nu}{3} & 0 & 0 \\ 0 & \alpha & 0 \\ 0 & 0 & 0 \end{bmatrix} \text{ and } \boldsymbol{T}^{-1} = \begin{bmatrix} -u_1 & 1 & 0 \\ u_1^2 - \frac{e_{\text{tot}}}{\rho} & -u_1 & 1 \\ 1 & 0 & 0 \end{bmatrix} \tag{52}$$

Here ν is the kinematic viscosity and α is the thermal diffusivity. We also transform the one-dimensional diffusion problem (50) using the matrix of left-eigenvectors $\boldsymbol{T}^{-1}$. The derivatives of $\boldsymbol{T}$ and $\boldsymbol{T}^{-1}$ are neglected. Hence, the transformed problem possess a diagonal diffusive matrix of real eigenvalues $\boldsymbol{D}$, which multiplies the derivative of the transformed unknowns. It can be checked that the transformed problem is dimensionally well defined, and that the scaling matrix can be defined as the identity matrix $\boldsymbol{M} = \boldsymbol{I}$ because products (31) are dimensionally correct.

Consequently, the spectrum of the transformed diffusion problem is:

$$\text{spec}_{M^{-1}}\left(\left(\frac{k_1^0 k_1^0}{h^2}\right)^2 \boldsymbol{D}^\top \boldsymbol{M}\boldsymbol{D}\right) = \left\{\left(\frac{k_1^0 k_1^0 4\nu}{h^2 3}\right)^2, \left(\frac{k_1^0 k_1^0 \alpha}{h^2}\right)^2, 0\right\}. \tag{53}$$

Note that each one of these eigenvalues may be an upper bound for the spectrum depending on the kinematic viscosity and thermal diffusion values. Therefore, we assure that the spectral radius of the transformed stabilization matrix problem:

$$\text{spec}_{M^{-1}}\left((\boldsymbol{\tau}')^{-1}\boldsymbol{M}(\boldsymbol{\tau}')^{-1}\right) = \left\{\left(\frac{1}{\tau'_\rho}\right)^2, \left(\frac{1}{\tau'_m}\right)^2, \left(\frac{1}{\tau'_{e_{\text{tot}}}}\right)^2\right\}, \tag{54}$$

Downloaded by Kungliga Tekniska Högskolan At 05:21 18 May 2016 (PT)

be greater than the spectral radius of (53) by forcing each one of the components to be:

$$\frac{1}{\tau'_\rho}=\frac{1}{\tau'_m}=\frac{1}{\tau'_{e_{\text{tot}}}}=a_m\frac{k_1^0k_1^04\nu}{h^23}+a_e\frac{k_1^0k_1^0\alpha}{h^2} \tag{55}$$

Here we have introduced a_m and a_e as parameters of the problem. After retrieving the transformation, we get the same values for all terms of the matrix of stabilization as the right hand side of (55). In practice, we make a_m and a_e zero for all terms, except for τ_m^{-1}, for which we choose $a_m=1$ and for τ_e^{-1}, for which we also guarantee $a_e=1$. That is, we define the matrix of stabilization for the one-dimensional diffusive term as:

$$\boldsymbol{\tau}^{-1}=\begin{bmatrix}0&0&0\\0&\tau_m^{-1}&0\\0&0&\tau_{e_{\text{tot}}}^{-1}\end{bmatrix},\ \text{with}\ \tau_m^{-1}=\frac{k_1^0k_1^04\nu}{h^23}\ \text{and}\ \tau_{e_{\text{tot}}}^{-1}=\frac{k_1^0k_1^0\alpha}{h^2}. \tag{56}$$

This approximation has been tested and shown to give good results, even though it is not the complete bound definition for the diffusive term.

3.3.3 Reactive term. In the case of the reactive-term contribution $\boldsymbol{SU}$, the one-dimensional reactive matrix is given by:

$$\boldsymbol{S}=\begin{bmatrix}0&0&0\\f_1&0&0\\r&f_1&0\end{bmatrix}, \tag{57}$$

where f_1 is the one-dimensional body source, and r is the heat source. This matrix must be scaled with a diagonal scaling matrix $\boldsymbol{Q}$, which can be designed for convenience using reference scaling values. At this point we can note that the scaling matrix $\boldsymbol{Q}=\text{diag}(c^4,c^2,1)$, with the acoustic speed c, gives a dimensionally well defined product $[\boldsymbol{U}^\top\boldsymbol{QSU}]=M^2L^{-2}T^{-5}$. From now on, let $\boldsymbol{U}$, $\boldsymbol{V}$ be elements in the domain of the scaled matrix $\boldsymbol{QS}$ and $\boldsymbol{G},\boldsymbol{H}$ elements in its range. The scaling matrix $\boldsymbol{M}=\text{diag}(c^{-6},c^{-4},c^{-2})$ makes products (31) correct. If we make the product $\boldsymbol{G}^\top\boldsymbol{MH}$, it gives the correct dimensional terms $[\rho^2u_1^{10}h^{-2}c^{-6}]=[\rho^2u_1^8h^{-2}c^{-4}]=[\rho^2u_1^6h^{-2}c^{-2}]=M^2L^2T^{-4}$. The product $\boldsymbol{U}^\top\boldsymbol{M}^{-1}\boldsymbol{V}$ is also correct since $[\rho^2c^6]=[\rho^2u_1^2c^4]=[\rho^2u_1^4c^2]=M^2L^6T^{-6}$.

Hence, we can calculate the spectrum of the scaled reactive term as:

$$\text{spec}_{M^{-1}}\left((\boldsymbol{QS})^\top\boldsymbol{MQS}\right)=\left\{\frac{r^2+2c^2f_1^2+\sqrt{r^4+4c^2f_1^2r^2}}{2c^8},\frac{r^2+2c^2f_1^2-\sqrt{r^4+4c^2f_1^2r^2}}{2c^8},0\right\}. \tag{58}$$

Likewise, the spectrum of the scaled matrix of stabilization parameters problem is:

$$\text{spec}_{M^{-1}}\left(\boldsymbol{Q\tau}^{-1}\boldsymbol{MQ\tau}^{-1}\right)=\left\{\left(\frac{\tau_\rho^{-1}}{c^2}\right)^2,\left(\frac{\tau_m^{-1}}{c^2}\right)^2,\left(\frac{\tau_{e_{\text{tot}}}^{-1}}{c^2}\right)^2\right\}. \tag{59}$$

Downloaded by Kungliga Tekniska Högskolan At 05:21 18 May 2016 (PT)

Downloaded by Kungliga Tekniska Högskolan At 05:21 18 May 2016 (PT)

We can fulfill the condition of equating the spectral radius of both problems by making each eigenvalue of (59) be equal to the first eigenvalue of (58). As a result, the matrix of stabilization is defined for the one-dimensional reactive term as:

$$\boldsymbol{\tau}^{-1} = \begin{bmatrix} \tau_\rho^{-1} & 0 & 0 \\ 0 & \tau_m^{-1} & 0 \\ 0 & 0 & \tau_{e_{\text{tot}}}^{-1} \end{bmatrix}, \text{with, } \tau_\rho^{-1} = \tau_m^{-1} = \tau_{e_{\text{tot}}}^{-1}$$

$$= \left(\frac{r^2 + 2c^2 f_1^2 + \sqrt{r^4 + 4c^2 f_1^2 r^2}}{2c^4} \right)^{1/2}. \tag{60}$$

3.3.4 Extension to multiple dimensions. Finally, we can extend the one-dimensional analysis in order to approximate the multi-dimensional stabilization matrix. Let us denote by $\boldsymbol{k}^0$ the multi-dimensional vector of algorithmic parameters $[\boldsymbol{k}^0] = k_i^0, 1 \leqslant i \leqslant d$, where k_i^0 is the algorithmic parameter in the ith direction. We propose to apply the one-dimensional momentum stabilization parameter equally into all dimensions of the momentum equation. Therefore, the stabilization matrix for multiple dimensions can be computed as:

$$\boldsymbol{\tau}^{-1} = \begin{bmatrix} \tau_\rho^{-1} & \mathbf{0}^\top & 0 \\ \mathbf{0} & \tau_m^{-1}\boldsymbol{I} & \mathbf{0} \\ 0 & \mathbf{0}^\top & \tau_{e_{\text{tot}}}^{-1} \end{bmatrix}, \tag{61}$$

with $\mathbf{0}$ being the vector of $\mathbb{R}^d$ with zero in all its components and:

$$\tau_\rho^{-1} = \frac{C_2(|\boldsymbol{u}| + c)}{h} + C_3 \left(\frac{r^2 + 2c^2|\boldsymbol{f}|^2 + \sqrt{r^4 + 4c^2|\boldsymbol{f}|^2 r^2}}{2c^4} \right)^{1/2}, \tag{62}$$

$$\tau_m^{-1} = \frac{C_1}{h^2}\frac{4\nu}{3} + \frac{C_2(|\boldsymbol{u}| + c)}{h} + C_3 \left(\frac{r^2 + 2c^2|\boldsymbol{f}|^2 + \sqrt{r^4 + 4c^2|\boldsymbol{f}|^2 r^2}}{2c^4} \right)^{1/2}, \tag{63}$$

$$\tau_{e_{\text{tot}}}^{-1} = \frac{C_1 \alpha}{h^2} + \frac{C_2(|\boldsymbol{u}| + c)}{h} + C_3 \left(\frac{r^2 + 2c^2|\boldsymbol{f}|^2 + \sqrt{r^4 + 4c^2|\boldsymbol{f}|^2 r^2}}{2c^4} \right)^{1/2}. \tag{64}$$

In these expresions C_1, C_2 and C_3 are algorithmic parameters. The algorithmic parameter C_1 approximates $|\boldsymbol{k}^0|^2$. On the other hand, the algorithmic constant C_2 approximates the $|\boldsymbol{k}^0|$ multiplied by the cosine of the angle formed by $\boldsymbol{k}^0$ and $\boldsymbol{u}$. The reactive contribution is multiplied by the algorithmic constant C_3. In this work we take $C_1 = 12p^2$, $C_2 = 2p$ and $C_3 = 1$, where p is the order of the finite

element interpolation. The matrix of stabilization parameters depends on velocity and the acoustic speed. This non-linearity $\boldsymbol{\tau}(\boldsymbol{U})$ is also considered for non-linear subscales.

3.4 Shock capturing technique

The previous stabilized finite element formulation yields a globally stable solution but does not guarantee stability in the presence of sharp gradients of the solution.

Indeed, gradients of the solution may appear in the supersonic compressible flow in the form of transonic shocks. Consequently, the globally stabilized formulation requires to be complemented with a shock capturing technique in order to yield stability and convergence in the entire domain. The main idea of such a shock capturing technique is to increase the amount of numerical dissipation in the proximity of sharp gradients. The method adds some artificial kinematic viscosity ν_{SC} and thermal diffusivity α_{SC} into the diffusive Galerkin term of the finite element Equation (22). We aim to introduce the numerical diffusion in such way that we modify diffusion in the momentum and energy equations, but avoiding the modification of the mass equation.

We consider two non-linear methods in order to calculate the added diffusion values. The first non-linear method that we implement is a residual-based technique, which is consistent, in the sense that if it is applied to the exact solution $\boldsymbol{U}$, the added diffusion is zero. For this technique we calculate the artificial kinematic viscosity using:

$$\nu_{\mathrm{SC}} = \left(\frac{1}{2}C_a h\right)\frac{\left|\boldsymbol{R}_{\boldsymbol{m}}(\boldsymbol{U}, \boldsymbol{U}_h)\right|}{|\nabla \boldsymbol{m}_h|} \quad \text{if } |\nabla \boldsymbol{m}_h| \neq 0,\ \nu_{\mathrm{SC}} = 0 \quad \text{otherwise}, \tag{65}$$

where C_a is an algorithmic constant, h is the characteristic length that gives dimensional consistency to the expresion, and $|\nabla \boldsymbol{m}_h|$ is the Frobenius norm of the gradient of the finite element solution for momentum. Similarly, for the artificial thermal diffusivity we use:

$$\alpha_{\mathrm{SC}} = \left(\frac{1}{2}C_a h\right)\frac{\left|\boldsymbol{R}_{e_{\mathrm{tot}}}(\boldsymbol{U}, \boldsymbol{U}_h)\right|}{\left|\nabla e_{\mathrm{tot},h}\right|} \quad \text{if } \left|\nabla e_{\mathrm{tot},h}\right| \neq 0, \alpha_{\mathrm{SC}} = 0 \quad \text{otherwise}. \tag{66}$$

In the previous equation, $|\nabla e_{\mathrm{tot},h}|$ is the norm of the gradient of the finite element solution for the total energy.

The second non-linear method is the weakly consistent orthogonal projection technique (Codina, 2011), which adds artificial diffusion only in the regions where sharp gradients are present. The orthogonal projection technique makes the added diffusion proportional to the projection of the gradient of the solution onto the space defined to be orthogonal to the finite element space, that is to say, we take the artificial viscosity as:

$$\nu_{\mathrm{SC}} = \left(\frac{1}{2}C_a |\boldsymbol{u}| h\right)\frac{\left|\boldsymbol{P}_h^{\perp}(\nabla \boldsymbol{m}_h)\right|}{|\nabla \boldsymbol{m}_h|} \quad \text{if } |\nabla \boldsymbol{m}_h| \neq 0, \nu_{\mathrm{SC}} = 0 \quad \text{otherwise}. \tag{67}$$

The norm of the velocity $|\boldsymbol{u}|$ gives dimensional consistency to the orthogonal projection-based calculation. In this method we calculate the artificial thermal diffusivity as:

$$\alpha_{\mathrm{SC}} = \left(\frac{1}{2}C_a |\boldsymbol{u}| h\right)\frac{\left|\boldsymbol{P}_h^{\perp}\left(\nabla e_{\mathrm{tot},h}\right)\right|}{\left|\nabla e_{\mathrm{tot},h}\right|} \quad \text{if } \left|\nabla e_{\mathrm{tot},h}\right| \neq 0,\ \alpha_{\mathrm{SC}} = 0 \quad \text{otherwise}. \tag{68}$$

Downloaded by Kungliga Tekniska Högskolan At 05:21 18 May 2016 (PT)

Downloaded by Kungliga Tekniska Högskolan At 05:21 18 May 2016 (PT)

The value used in this work for the algorithmic constant is $C_a = 0.8$ for both residual and orthogonal projection methods (see Section 5 for the disscusion about this value).

In practice, the way to introduce the added numerical diffusion into the diffusive Galerkin term is to compute a modified viscous stress tensor $\check{\boldsymbol{\tau}} = [\tau_{ij}]$ and heat flux vector $\check{\boldsymbol{q}} = [q_i]$. Within the modification of those tensors, we propose two distinct ways which are explained below. Figure 1 presents the main idea of how the artificial diffusion is added by each method.

The first method is the so-called isotropic method, which is based on the addition of the artificial diffusion into all the components of the viscous stress tensor and heat flux vector, that is:

$$\check{\tau}_{ij} = \left(1+\frac{\rho \nu_{\mathrm{SC}}}{\mu}\right)\tau_{ij} \quad \text{and} \quad \check{q}_i = \left(1+\frac{\rho c_v \alpha_{\mathrm{SC}}}{\lambda}\right)q_i. \tag{69}$$

The second method that we propose is to add the numerical diffusion in an anisotropic fashion. The anisotropic diffusion method consists in the addition of the artificial diffusion into the streamline direction ν_{ST} and α_{ST}, excluding the already incorporated variational multi-scale stabilization diffusion quantity, which we roughly estimate as:

$$\nu_{\mathrm{SG}} = \tau_m |\boldsymbol{u}|^2 \quad \text{and} \quad \alpha_{\mathrm{SG}} = \tau_{e_{\mathrm{tot}}} |\boldsymbol{u}|^2, \tag{70}$$

but, not decreasing the stabilization:

$$\nu_{\mathrm{ST}} = \max(0, \nu_{\mathrm{SC}} - \nu_{\mathrm{SG}}) \quad \text{and} \quad \alpha_{\mathrm{ST}} = \max(0, \alpha_{\mathrm{SC}} - \alpha_{\mathrm{SG}}). \tag{71}$$

Moreover, as explained by (Codina, 1993), the shock capturing artificial diffusion should be introduced in the crosswind direction. This is done by adding the artificial diffusion with anisotropic tensors.

In order to introduce the artificial thermal diffusion into the heat flux vector, we use an anisotropic second-order tensor of the form:

$$\check{q}_i = \left(\delta_{ij} + \frac{\rho c_v \alpha_{\mathrm{SC}}}{\lambda} O_{ij} + \frac{\rho c_v \alpha_{\mathrm{ST}}}{\lambda} S_{ij}\right) q_j, \tag{72}$$

where the anisotropic tensor is defined in terms of the second-order projector into the streamline direction $S_{ij}(m_i m_j / |m|^2)$, and in terms of the orthogonal projector $O_{ij} = \delta_{ij} - S_{ij}$. We also include the artificial viscosity into the viscous stress tensor using a fourth-order anisotropic tensor:

$$\check{\tau}_{ij} = \left(\delta_{ij}\delta_{kl} + \frac{\rho \nu_{\mathrm{SC}}}{\mu} O_{ijkl} + \frac{\rho \nu_{\mathrm{ST}}}{\mu} S_{ijkl}\right) \tau_{kl}. \tag{73}$$

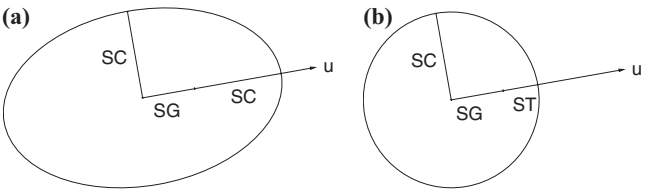

Figure 1.
Shock capturing methods

Notes: (a) Isotropic diffusion ellipse; (b) anisotropic diffusion ellipse

here $\boldsymbol{I}=[\delta_{ij}\delta_{kl}]$ stands for the fourth-order identity tensor. We exploit the symmetric property of the viscous stress tensor in order to construct the fourth-order orthogonal $\boldsymbol{O}=[O_{ijkl}]$ and streamline $\boldsymbol{S}=[S_{ijkl}]$ tensors. First, we write the viscous stress tensor using Voigt's notation for the most general three-dimensional case:

$$\boldsymbol{\tau}=\begin{bmatrix}\tau_{11} & \tau_{12} & \tau_{13}\\ \tau_{21} & \tau_{22} & \tau_{23}\\ \tau_{31} & \tau_{32} & \tau_{33}\end{bmatrix}\equiv\begin{bmatrix}\tau_1 & \tau_6 & \tau_5\\ \tau_6 & \tau_2 & \tau_4\\ \tau_5 & \tau_4 & \tau_3\end{bmatrix}\rightarrow\boldsymbol{\tau}=(\tau_1,\tau_2,\tau_3,\tau_4,\tau_5,\tau_6)^{\top}. \tag{74}$$

Then, after some algebraic operations the nine independent elements of the fourth-order orthotropic streamline tensor can be written using Voigt's notation as follows:

$$\boldsymbol{S}=\begin{bmatrix}\frac{m_1m_1}{|\boldsymbol{m}|^2} & \frac{m_1m_2}{|\boldsymbol{m}|^2} & \frac{m_1m_3}{|\boldsymbol{m}|^2} & 0 & 0 & 0\\ \frac{m_1m_2}{|\boldsymbol{m}|^2} & \frac{m_2m_2}{|\boldsymbol{m}|^2} & \frac{m_2m_3}{|\boldsymbol{m}|^2} & 0 & 0 & 0\\ \frac{m_1m_3}{|\boldsymbol{m}|^2} & \frac{m_2m_3}{|\boldsymbol{m}|^2} & \frac{m_3m_3}{|\boldsymbol{m}|^2} & 0 & 0 & 0\\ 0 & 0 & 0 & \frac{m_2m_3}{|\boldsymbol{m}|^2} & 0 & 0\\ 0 & 0 & 0 & 0 & \frac{m_1m_3}{|\boldsymbol{m}|^2} & 0\\ 0 & 0 & 0 & 0 & 0 & \frac{m_1m_2}{|\boldsymbol{m}|^2}\end{bmatrix}. \tag{75}$$

The orthogonal projection is calculated according to the fourth-order definition $O_{ijkl}=\delta_{ij}\delta_{kl}-S_{ijkl}$ and is presented below using Voigt's notation:

$$\boldsymbol{O}=\begin{bmatrix}1-\frac{m_1m_1}{|\boldsymbol{m}|^2} & -\frac{m_1m_2}{|\boldsymbol{m}|^2} & -\frac{m_1m_3}{|\boldsymbol{m}|^2} & 0 & 0 & 0\\ -\frac{m_1m_2}{|\boldsymbol{m}|^2} & 1-\frac{m_2m_2}{|\boldsymbol{m}|^2} & -\frac{m_2m_3}{|\boldsymbol{m}|^2} & 0 & 0 & 0\\ -\frac{m_1m_3}{|\boldsymbol{m}|^2} & -\frac{m_2m_3}{|\boldsymbol{m}|^2} & 1-\frac{m_3m_3}{|\boldsymbol{m}|^2} & 0 & 0 & 0\\ 0 & 0 & 0 & 1-\frac{m_2m_3}{|\boldsymbol{m}|^2} & 0 & 0\\ 0 & 0 & 0 & 0 & 1-\frac{m_1m_3}{|\boldsymbol{m}|^2} & 0\\ 0 & 0 & 0 & 0 & 0 & 1-\frac{m_1m_2}{|\boldsymbol{m}|^2}\end{bmatrix}. \tag{76}$$

3.5 Explicit time integration

At this point we have described the space discrete stabilized finite element formulation. Let us now comment how we discretize in time.

We partition the time interval $(0,\ T)$ in a sequence of discrete time steps $0=t^0<t^1<,\ldots,<t^N=T$, with $\delta t>0$ the time step size defining $t^{n+1}=t^n+\delta t$ for $n=0,1,2,\ldots,N$. We also partition each time step into intermediate stages $t^n<t_1<t_2<,\ldots,<t^{n+1}$, S being the number of stages, which are considered to have a constant size for simplicity. Let us use the superscript to denote the time step counter and the subscript to denote the intermediate stage counter.

Downloaded by Kungliga Tekniska Högskolan At 05:21 18 May 2016 (PT)

Downloaded by Kungliga Tekniska Högskolan At 05:21 18 May 2016 (PT)

Let us describe the transient-term integration of the finite element problem (22). After assembling the elemental contributions of the space discrete stabilized finite element problem, the discrete matrix form of the transient problem can be written as:

$$M\dot{\mathrm{U}} = \mathrm{R}(\mathrm{U}), \tag{77}$$

where U is the array that contains the nodal unknowns, M is the mass matrix, and R(U) is the residual of the discrete stabilized finite element problem. Solving this system of equations in an implicit fashion can be computationally very expensive. Our various applications of the compressible formulation, some of which require the solution of small spatial and temporal scales (such as turbulent flows and aeroacoustics problems), have prompted us to implement explicit time integration schemes which are reasonably in line with these needs. Therefore, we use an explicit time integration scheme in order to integrate the temporal derivatives, more precisely, we implement the family of explicit RK methods. For any number of stages, the finite element solution at t^{n+1} is given by the quadrature:

$$\mathrm{U}^{n+1} = \mathrm{U}^{n} + \mathrm{M}^{-1}\delta t \sum_{i=1}^{S} \mathrm{b}_i K_i, \tag{78}$$

where M^{-1} is the inverted mass matrix and K_i (for $1 \leqslant i \leqslant S$) are stage increments based on the evaluation of the space discrete stabilized finite element residual:

$$K_i = R\left(U^{n} + M^{-1}\delta t \sum_{j=1}^{i-1} \mathrm{a}_{ij} K_j\right). \tag{79}$$

Moreover, we calculate the time integration method for the temporal derivative of the dynamic subscales exploiting the explicit RK scheme adopted for the finite element equation, that is, we solve the subscales at time t^{n+1} with:

$$\widetilde{\boldsymbol{U}}^{n+1} = \widetilde{\boldsymbol{U}}^{n} + \delta t \sum_{i=1}^{S} b_i \widetilde{\boldsymbol{K}}_i. \tag{80}$$

The subscales at the intermediate stage t_i, which are also incorporated in the time integration stage of the finite element equation, are calculated as follows:

$$\widetilde{\boldsymbol{U}}^{t_i} = \widetilde{\boldsymbol{U}}^{n} + \delta t \sum_{j=1}^{i-1} \mathrm{a}_{ij} \widetilde{\boldsymbol{K}}_j, \tag{81}$$

where $1 \leqslant j < i \leqslant S$. The intermediate increments of the subscales transient equation are evaluated explicitly at t_j with the subscales residual:

$$\widetilde{\boldsymbol{K}}_j = \widetilde{\boldsymbol{P}}\left[\boldsymbol{R}\left(\boldsymbol{U}^{t_j}; \boldsymbol{U}_h^{t_j}\right)\right] - \boldsymbol{\tau}^{-1}\left(\boldsymbol{U}^{t_j}\right)\widetilde{\boldsymbol{U}}^{t_j}. \tag{82}$$

In the previous expresions, the non-linear subscales at the intermediate stage j are considered as $\boldsymbol{U}^{t_j} = \boldsymbol{U}_h^{t_j} + \widetilde{\boldsymbol{U}}^{t_j}$. As a final remark, we approximate the calculation of the non-linear subscales at intermediate stage j using the resulting values at the previous stage when the subscales are considered quasi-static, that is,

$\boldsymbol{U}^{t_j} = \boldsymbol{U}_h^{t_j} + \widetilde{\boldsymbol{U}}^{t_{j-1}}$. Expresions (78)-(81) depend on the definition of the coefficients a_{ij} (for $1 \leqslant j < i \leqslant S$) and b_i (for $1 \leqslant i \leqslant S$) for a specific RK method. In particular, we have implemented a four stages explicit RK method with coefficients:

$$a_{31} = a_{41} = a_{42} = 0, \quad a_{21} = \tfrac{1}{2}, \quad a_{32} = \tfrac{1}{2}, \quad a_{43} = 1,$$
$$b_1 = \tfrac{1}{6}, \quad b_2 = \tfrac{1}{3}, \quad b_3 = \tfrac{1}{3}, \quad b_4 = \tfrac{1}{6},$$

which is fourth-order in accuracy. This explicit method is subject to the Courant-Friedrich-Levi stability criterion for hyperbolic systems, which implies:

$$\frac{\delta t(|\boldsymbol{u}|+c)}{h} \leqslant 1, \tag{83}$$

as a necessary condition for numerical stability.

4. Numerical examples

In this section some numerical examples are presented. First, the three-dimensional lid-driven cavity problem is solved in order to demonstrate the multi-dimensional features of the proposed formulation. We also test including the body force and heat source into this problem. Then, we solve a periodic subsonic flow past a cylinder in order to assure the variational multi-scale stabilization. A convergence analysis is proposed for linear triangular elements. Finally, some compressible flow examples that exhibit supersonic shocks are solved in order to compare the proposed shock capturing methods. The flow is considered as an ideal gas in all cases, with ratio of specific heats $\gamma = 1.4$ and physical properties $c_p = 1.010$ kJ/(kg K) and $c_v = 0.718$ kJ/(kg K).

4.1 Three-dimensional lid-driven cavity

The three-dimensional lid-driven cavity problem is a widely used benchmark in computational fluid dynamics. The problem domain is a prismatic cavity $[0, L] \times [0, L] \times [0, L]$, with $L = 1$ m. The upper wall (x_1, x_2, L) m is constantly moving at a fixed velocity of $\boldsymbol{u}_w = (1, 0, 0)$ m/s, and the density is $\rho_w = 1$ kg/m^3. The temperature θ_w is also set over this boundary depending on the compressibility regime. A no-slip condition for velocity, an adiabatic condition for energy, and an impermeable condition for mass are set over the other walls.

In this problem we aim to test the multi-dimensional formulation including the convective, diffusive and source contributions into the compressible equations. For convenience, we include the orthogonal projection to the finite element residual, the time dependence, and the non-linearity of subscales. Comparissons are made by evaluating three Reynolds numbers, specifically $Re = 100$, $Re = 400$ and $Re = 1{,}000$. The Prandtl number is fixed to $Pr = 0.71$ for all cases. Flow conditions are laminar in all cases, and simulations are run until the stationary state is reached. The mesh is constituted by 64,000 hexahedral elements in a stuctured $40 \times 40 \times 40$ homogeneous distribution.

We first solve this problem without body force and heat source. This case is intended to compare our results with previous benchmarked solutions. To our knowledge, only incompressible results have been published in the case of a three-dimensional cubed-driven cavity (e.g. Albensoeder and Kuhlmann, 2005). Hence, in order to approximate the incompressibility condition the Mach number is fixed to a subsonic regime $M = 0.1$, and the temperature to $\theta_w = 0.2446$ K. Figure 2 shows the velocity profiles along the centerlines of the cavity. The compressible results are

Downloaded by Kungliga Tekniska Högskolan At 05:21 18 May 2016 (PT)

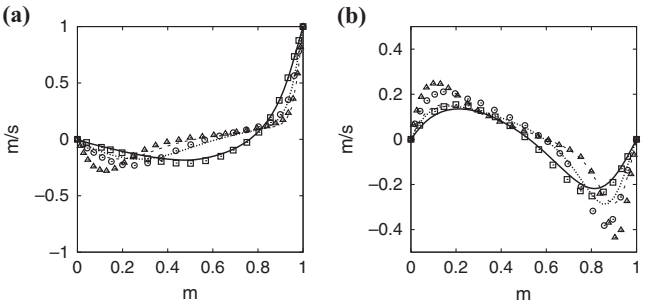

Notes: Compressible problem without source terms: (a) velocity profile along the centerline (0.5, 0.5, x_3); (b) velocity profile along the centerline (x_1, 0.5, 0.5). The Reynolds numbers are $Re = 100$ (solid line), $Re = 400$ (dotted line), and $Re = 1{,}000$ (dashed line). The symbols □ ($Re = 100$), ○ ($Re = 400$), △ ($Re = 1{,}000$) represent the extracted results from Albensoeder and Kuhlmann (2005)

Figure 2.
Three-dimensional lid-driven cavity results

Downloaded by Kungliga Tekniska Högskolan At 05:21 18 May 2016 (PT)

qualitatively in good agreement with previous numerical and experimental investigations, even if a comparisson is made with the incompressible results obtained by Albensoeder and Kuhlmann (2005). Compressible results are accurate in the location of the maximum and minimum velocities. However, the magnitude of the extremal values of the velocity differ substantially. This difference can be explained by the physics of the compressible Navier-Stokes equations.

We then include body force and heat source into the problem. For academic purposes, the body force is set to $\boldsymbol{f} = 0, 0, -0.1\ \mathrm{m/s^2}$. The heat source is also maintained homogeneus and constant $r = 1\ \mathrm{m^2/s^3}$. For this case, compressibility is fixed by setting $M = 1$, therefore, $\theta = 0.0024\ \mathrm{K}$. Figure 3 shows the velocity and temperature profiles along the centerlines of the cavity. The numerical behavior of the proposed stabilized formulation including source terms is appropriate. Smooth solutions are obtained for all Reynolds numbers. Some dissipation can be observed for the location and magnitude of the extremal velocities, when compared to the solution without including sources. Moreover, temperature results prove the correct solution for the heat and momentum equations.

The previous results assure a correct spatial integration given by the variational multi-scale finite element formulation. That is, we guarantee a correct definition for the matrix τ of stabilization parameters, but also demonstrate the multi-dimensional capability of the variational formulation. Because there is not a dynamical behavior for this laminar problem, we solve the following numerical example in order to test the time integration of finite element scales and subscales.

4.2 Subsonic flow past a cylinder at Re = 100 and M = 0.5

The problem is defined by a cylinder infinitely long in the axial direction, which is immersed in compressible fluid and is subject to an uniform incident flow. The flow over the cylinder is solved as a bidimensional problem, and it is intended to test the proposed variational multi-scale stabilized formulations on a dynamical problem. We restrict the flow to the subsonic range in order to avoid the need of the shock capturing techniques.

The problem domain is $[0, L] \times [-H/2, H/2]$ with $L = 7\ \mathrm{m}$ and $H = 2.4\ \mathrm{m}$, with the cylinder diameter $D = 0.2\ \mathrm{m}$ centered at point $(0.8, 0)\ \mathrm{m}$. Boundary conditions are

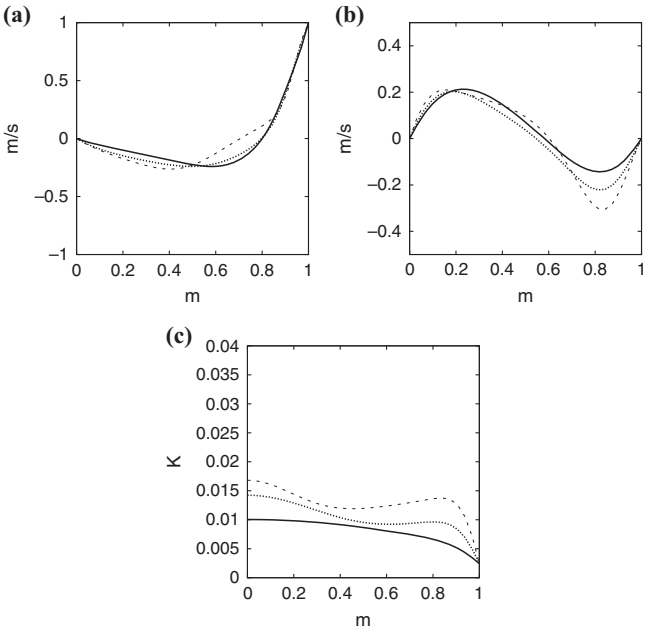

Notes: Compressible problem including source terms: (a) velocity profile along the centerline (0.5, 0.5, x_3); (b) velocity profile along the centerline (x_1, 0.5, 0.5); (c) temperature profile along the centerline (0.5, 0.5, x_3). The Reynolds numbers are $Re = 100$ (solid line), $Re = 400$ (dotted line), and $Re = 1{,}000$ (dashed line)

Figure 3.
Three-dimensional lid-driven cavity results

set as follows. The flow is injected from the left wall with uniform constant velocity $\boldsymbol{u}_{in} = (1,0)$ m/s, temperature $\theta_{in} = 9.73\times10^{-3}$ K, and density $\rho_{in} = 1$ kg/m^3. Over the adiabatic upper and lower walls symmetric boundary conditions are imposed, with vertical component of velocity and horizontal component of the stress imposed to zero. On the cylinder surface Γ_w, a no-slip condition for velocity is imposed. Over the outflow wall, density is set to $\rho_{out} = 1$ kg/m^3; zero stress and adiabatic conditions are considered for the subsonic flow. The viscosity and heat conductivity are $\mu = 0.002$ kg/(m s) and $\lambda = 2.8676$ kJ/(m K s), respectively.

Three different unstructured meshes composed of P_1 elements are used to solve this problem. These meshes, shown in Figure 4, are generated defining the mesh size $h_k = h_0/2^k$ in terms of sucesive divisions k. The mesh of Figure 4(a) is defined with $h_0 = 0.05$ m and 14,008 elements; the mesh of Figure 4(b) is defined as half the size of the mesh of Figure 4(a), that is, $h_1 = 0.025$ m with 54,884 elements; furthermore, the mesh of Figure 4(c) is defined as half the size of the mesh of Figure 4(b) as $h_2 = 0.0125$ m, with 217,162 elements. The time step size of the explicit fourth-order RK time integration scheme is set to a constant $t = 0.001$ s value for all simulations. This time step size is for all simulations lower than the explicit restriction given by the problem.

We use this numerical example to compare the proposed variational multi-scale stabilized finite element formulation. That is, we evaluate the numerical behavior of subscales, which can be defined orthogonal to the finite element residual space, dynamic, or can be incorporated in all the non-linear terms. The following notation is

Downloaded by Kungliga Tekniska Högskolan At 05:21 18 May 2016 (PT)

Downloaded by Kungliga Tekniska Högskolan At 05:21 18 May 2016 (PT)

used in order to clarify the different subscales definition in the numerical example. Defining the space where the subscales live as orthogonal to the finite element residual space is denoted by the "O" letter, otherwise defining it as the finite element residual space is denoted as "F." The letter "D" is used for dynamic subscales, and for the quasi-static definition of the subscales the letter "Q" is employed. Finally, if the subscales are included in the non-linear terms the letter "N" is used, and if they are not considered, the letter "L" is used.

Smooth result fields are obtained for the variational multi-scale formulation using the meshes presented above. The periodic transient solution for the $Re = 100$ case, which has been reported previously (Hauke and Hughes, 1998; Mittal and Tezduyar, 1998), is obtained in correspondence with the wake oscillations. All the simulations are run until the mean values of the forces exerted by the fluid over the cylinder reach a statistically stationary state. Due to the temporal dependence of the solution, we restrict the presentation of contour results to a given time step. Pressure, temperature, and velocity magnitude contours at a given instant of the flow are shown in Figure 5. These results are obtained with the ODN method using the mesh of Figure 4(c). Solutions obtained with other subscales definitions, that we do not present for conciseness, give qualitatively similar contour results. Instead, some calculations are performed in order to quantify the numerical results obtained with the proposed formulations. We calculate the non-dimensional Strouhal number:

$$\mathrm{St} = \frac{\mathrm{f}_f D}{|\boldsymbol{u}_{in}|}, \tag{84}$$

based on the cylinder diameter D and the frequency of the wake oscillations f_f. In addition, the non-dimensional drag and lift coefficients:

$$\mathrm{C_d} = -\frac{F_1}{\frac{1}{2}\rho_{in}|\boldsymbol{u}_{in}|^2 D}, \mathrm{C_l} = \frac{F_2}{\frac{1}{2}\rho_{in}|\boldsymbol{u}_{in}|^2 D}, \tag{85}$$

are calculated using the exerted force of the fluid over the cylinder:

$$\boldsymbol{F} = \int_{\Gamma_w} -\left(-p\boldsymbol{I} + 2\mu\nabla^S \boldsymbol{u} - \frac{2}{3}\mu(\nabla\cdot\boldsymbol{u})\boldsymbol{I}\right)\cdot\boldsymbol{n} \; d\Gamma. \tag{86}$$

The time history of the non-dimensional drag an lift coefficients are shown in Figure 6 for the solution obtained with the ODN method, and the mesh of Figure 4(c).

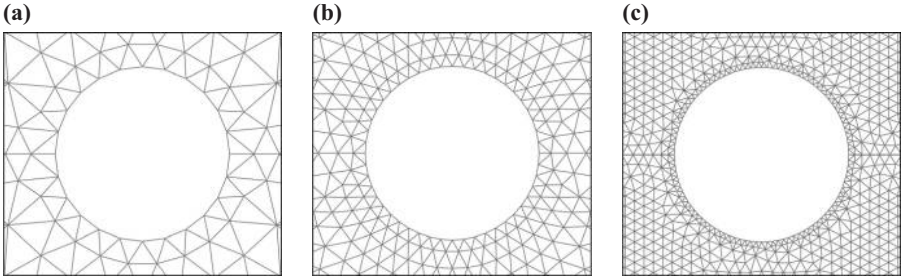

Figure 4.
Detail of three unstructured P_1 meshes used for the analysis of flow over a cylinder

Notes: (a) Mesh $h = 0.05$ m; (b) mesh $h = 0.025$ m; (c) mesh $h = 0.0125$ m

Downloaded by Kungliga Tekniska Högskolan At 05:21 18 May 2016 (PT)

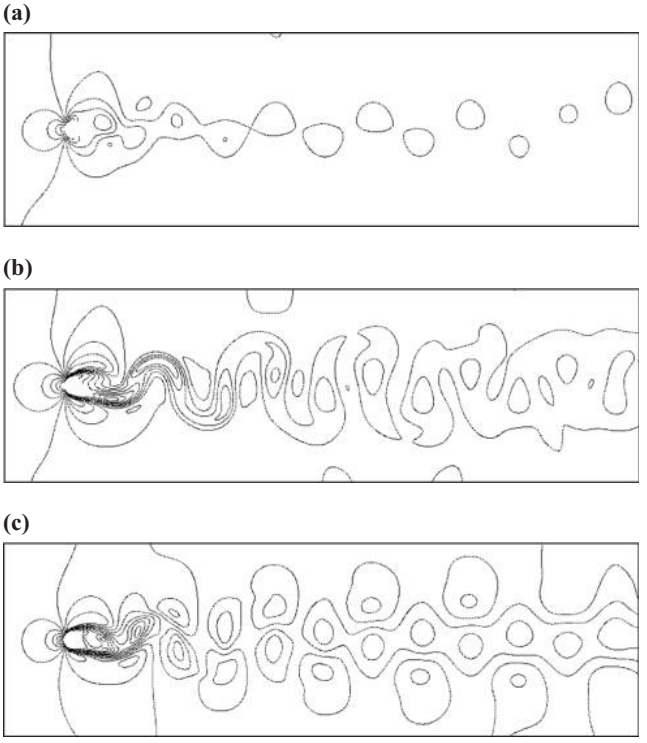

Notes: (a) Pressure; (b) temperature; (c) velocity magnitude calculated with the mesh of Figure 4(c). Results are obtained with the subscales defined as ODN

Figure 5.
Instantaneous contour fields of flow over a cylinder

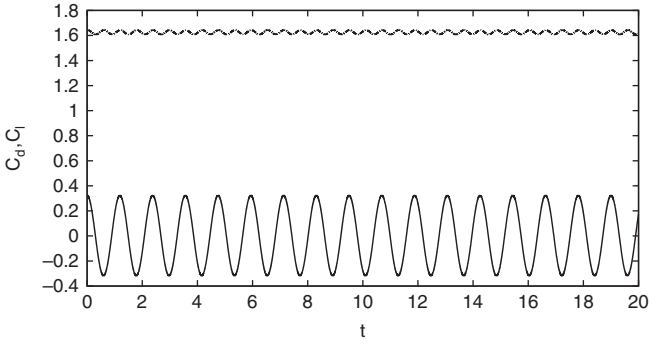

Notes: Lift (solid line) and drag (dashed line) results are calculated using the mesh of Figure 4(c), and defining the subscales as ODN

Figure 6.
Time history of drag and lift coefficients for the subsonic flow past a cylinder

We propose to calculate the convergence of the proposed formulations by using the discrete L^p-norm. Since the flow over a cylinder problem does not posess an analytical solution, the following convergence analysis is proposed. For a fixed time t, the L^p-norm of a discrete solution $u_h(\boldsymbol{x}, h, \delta t)$ can be written as the composition of the L^p-norm of the

analytical solution $u(\boldsymbol{x})$ plus some time and spatial integration dependent terms. If we set a constant time step size and the mesh size is defined in terms of consecutive divisions, we can write those discrete L^p-norms of the discrete solution as:

$$\left\|u_h(\boldsymbol{x}, h_k, \delta t)\right\|_p \approx \left\|u(\boldsymbol{x})\right\|_p + c_1(\delta t)^r + c_2(h_k)^q, \quad k = 0, 1, 2. \tag{87}$$

Consequently, the calculation of the quotient between consecutive differences of the L^p-norm:

$$\mathcal{Q} = \frac{\left|\left\|u_h(\boldsymbol{x}, h_0, \delta t)\right\|_p - \left\|u_h(\boldsymbol{x}, h_1, \delta t)\right\|_p\right|}{\left|\left\|u_h(\boldsymbol{x}, h_1, \delta t)\right\|_p - \left\|u_h(\boldsymbol{x}, h_2, \delta t)\right\|_p\right|}, \tag{88}$$

and the substitution of mesh size definitions into the previous quotient:

$$\mathcal{Q} = \frac{c_2 h_0^q \left(1 - \frac{1}{2^q}\right)}{c_2 h_0^q \left(\frac{1}{2^q} - \frac{1}{2^{2q}}\right)} = \frac{2^{2q} - 2^q}{2^q - 1} = 2^q, \tag{89}$$

makes possible to get an expresion for the convergence order q of the spatial integration term:

$$\log_2 \mathcal{Q} = q. \tag{90}$$

Time L^∞-norm of Strouhal numbers and time average of drag coefficients are presented in Tables I-II, respectively. The convergence order q is also presented in these tables for the calculated values. It can be observed that both the time L^∞-norm of Strouhal numbers, and time average of drag coefficients converge to a greater value as the mesh size is refined. Our results agree with the previously reported Strouhal number values [0.167, 0.17] for the vortex shedding (Mittal and Tezduyar, 1998). This characteristic can be used together with the convergence order in order to compare the stabilization methods.

Mesh	SUPG	FQL	FQN	FDL	FDN	OQL	OQN	ODL	ODN
$h = 0.05$	0.1518	0.1527	0.1515	0.1539	0.1523	0.1523	0.1516	0.1523	0.1515
$h = 0.025$	0.1646	0.1647	0.1642	0.1654	0.1644	0.1652	0.1650	0.1652	0.1650
$h = 0.0125$	0.1673	0.1675	0.1670	0.1680	0.1675	0.1684	0.1683	0.1684	0.1683
q	2.2193	2.1142	2.1384	2.1192	2.0035	2.0190	2.0075	2.0190	2.0193

Table I. Subsonic flow past a cylinder results

Note: Time L^∞-norm of Strouhal number

Mesh	SUPG	FQL	FQN	FDL	FDN	OQL	OQN	ODL	ODN
$h = 0.05$	1.3615	1.3853	1.3377	1.4008	1.3536	1.4108	1.3938	1.4106	1.3935
$h = 0.025$	1.5160	1.5317	1.5044	1.5407	1.5112	1.5321	1.5270	1.5321	1.5267
$h = 0.0125$	1.6053	1.6140	1.6013	1.6191	1.6052	1.6277	1.6257	1.6277	1.6257
q	0.7908	0.8309	0.7826	0.8354	0.7455	0.3434	0.4324	0.3458	0.4280

Table II. Subsonic flow past a cylinder results

Note: Time average of non-dimensional drag coefficient

Downloaded by Kungliga Tekniska Högskolan At 05:21 18 May 2016 (PT)

Downloaded by Kungliga Tekniska Högskolan At 05:21 18 May 2016 (PT)

Defining the subscales as orthogonal to the finite element space gives the most well approximated solutions. The results given by the calculated norms, both for the Strouhal number and for the drag coefficient indicate a less-dissipative behavior of this method, compared to the finite element residual definition for the space of subscales. However, the convergence order is lower for the orthogonal subscales. Moreover, including the time-dependency of the subscales improves the accuracy of the subscales defined in the finite element residual space. The solution obtained by FDL method gives accurate results together with a high convergence order. This method is more accurated in the drag results than the former stabilization SUPG method, and its convergence order is higher.

On the contrary, non-linear contribution of subscales reduces a little the accuracy for both the subscales defined in the finite element residual space, and for the orthogonal subscales. The combination between orthogonal, non-linear and dynamic subscales gives a highly accurate method. Nonetheless, the convergence order for this method is not the highest for the element sizes considered.

4.3 $M = 2.9$ inviscid shock reflection

We evaluate next the shock capturing methods by solving the inviscid shock reflection problem at $M = 2.9$. The supersonic reflected shock problem is widely used in order to test the compressible flow solvers. We also exploit this numerical example so that high-order approximations are tested. For solving this problem we use the variational multi-scale stabilization formulation defining the space of subscales orthogonal to the finite element residual space, and considering the time dependence and non-linear contribution of subscales.

The problem domain is $[0, L] \times [-H/2, H/2]$, with $L = 4.1$ m and $H = 0.5$ m. The flow is injected from the left and upper walls. Over the inlet left wall the Mach number is set to $M = 3$, hence, fixed values of velocity $(2.9, 0)$ m/s, density 1 kg/m^3, and temperature 0.00247 K are set. Over the upper inlet wall the Mach number is $M = 2.378$, thus, fixed values of velocity $(2.6193, -0.5063)$ m/s, density 1.7 kg/m^3, and temperature 0.00311 K are also set. A slip condition for the velocity and an adiabatic condition for energy are set over the lower wall. Over the outflow wall no conditions need to be imposed because the flow is supersonic. The values of viscosity and conductivity are 0.

We use P_2 elements in order to solve a high-order approximation. Nonetheless, P_1 elements are used to compare the shock capturing techniques. In both cases the finite element mesh is composed by 13,120 triangular elements distributed in a structured non-symmetric fashion. This unstructured configuration is presented in Figure (7). All simulations are run until the steady state is reached considering the time step size given by the stability condition (3.5). Adequate physical solutions are found using both the residual-based and the orthogonal projection-based shock capturing methods. Overshoots are smoothed according to the benchmarked solutions (Mittal and Tezduyar, 1998; Rispoli and Saavedra, 2006; Tezduyar and Senga, 2006; Kotteda and

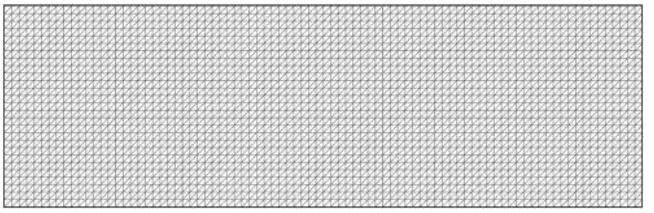

Figure 7.
Detail of the unstructured mesh configuration used for the inviscid shock reflection

Downloaded by Kungliga Tekniska Högskolan At 05:21 18 May 2016 (PT)

Mittal, 2014). Figure 8 shows the steady state contours for density and velocity magnitude solved with the anisotropic orthogonal projection-based shock capturing method and the mesh composed by P_2 elements.

The analysis of the solutions obtained by the isotropic and anisotropic, as well as the residual-based and the orthogonal projection-based shock capturing methods, is made by comparing the horizontal component of the velocity solution at $(x_1, 0.25)$ m. Figure 9 plots the solution obtained by the shock capturing methods for two distinct definitions of the algorithmic constant $C_a = 0.8$ and $C_a = 0.2$. These results are obtained with the mesh composed by P_1 elements. In Figure 9 the analytical solution presented by Mittal and Tezduyar (1998), together with the solution found without including the shock capturing method, are also plotted.

A correct solution for the problem is found with the anisotropic method and the $C_a = 0.8$ value. The anisotropic residual-based shock capturing method gives an accurate and less-diffusive solution than previous solutions obtained using the same mesh size (Tezduyar and Senga, 2006; Kotteda and Mittal, 2014). Because the anisotropic method adds the artificial diffusivity only in the crosswind direction, this method is less non-linear. In contrast, due to the high non-linearities in the problem introduced by the artificial diffusion of the isotropic method, this method only gives a stable solution with a lower $C_a = 0.2$ coefficient. With the lower $C_a = 0.2$ value, some overshoots in the solution obtained by both isotropic and anisotropic methods can be observed.

The orthogonal projection-based shock capturing method gives more diffusive results near the solution gradients, when compared to the residual-based method. However, the overall solution obtained by this technique is adequate and gives accurate results, when compared to the solution without a shock capturing method.

4.4 Supersonic flow past a cylinder at $Re = 2{,}000$ and $M = 2$

The supersonic flow past a cylinder problem at $Re = 2{,}000$ and $M = 2$ is presented as a benchmark problem in order to test the shock capturing techniques in a viscid supersonic case. The description of the problem is similiar to the subsonic flow past a

Figure 8.
Inviscid shock reflection results

Notes: (a) Density contour; (b) velocity magnitude contour. Solution is obtained using the anisotropic orthogonal projection-based shock capturing method

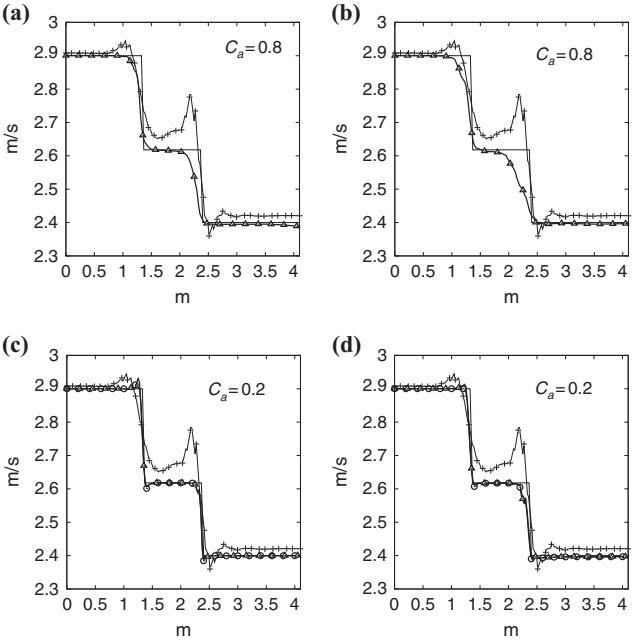

Notes: Horizontal velocity component at $(x_1, 0.25)$ m: Residual-based method used in (a) and (c); Orthogonal projection -based method used in (b) and (d); The solid line represents the analytical solution presented by Mittal and Tezduyar (1998). The solution obtained without shock capturing method is plotted using a solid marked line. Solid lines with symbols ○ (isotropic), and △ (anisotropic) represent the solution obtained using shock capturing methods

Figure 9.
Inviscid shock reflection solution

cylinder presented in subsection 4.2. In this supersonic case, an adiabatic condition is fixed over the cylinder surface and the physical conditions are set to $\mu = 0.0001$ kg/(m s) and $\lambda = 0.14338$ kJ/(m K s).

For this problem, we aim to test the ODN variational multi-scale formulation together with the anisotropic residual-based shock capturing technique, that give the best approximation for the inviscid reflected shock example. The finite element mesh consists of an unstructured mesh composed by 31,288 linear triangular elements. Smaller elements are used near the wall cylinder, whereas the mesh is coarser in the rest of the domain. The mesh size was fixed to $h = 0.005$ m in the finer region near the cylinder boundary. Due to the viscid condition of the problem, the solution is reached by setting the time step size lower than the explicit scheme stability condition (3.5). Figure 10 shows the solution for the supersonic flow over a cylinder solved using the ODN stabilization formulation, together with anisotropic residual-based shock capturing method.

Comparing this solution to the ones obtained in previous formulations, the fields are almost identical. The solution difers from the steady state solution obtained by Rispoli and Saavedra (2006) in the sense that no Sutherland law is used for viscosity in this example.

Downloaded by Kungliga Tekniska Högskolan At 05:21 18 May 2016 (PT)

Downloaded by Kungliga Tekniska Högskolan At 05:21 18 May 2016 (PT)

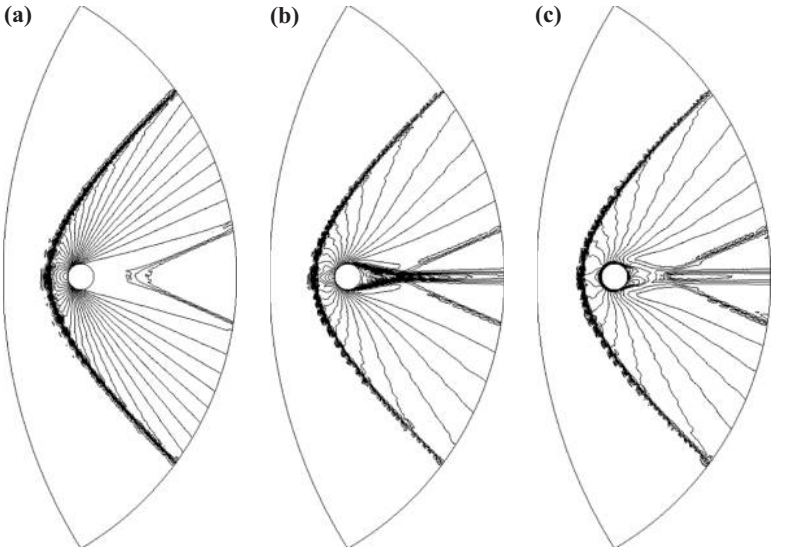

Figure 10.
Supersonic flow past a cylinder results

Notes: (a) Pressure contour; (b) velocity magnitude contour; (c) temperature contour. The solution is obtained using the ODN stabilization formulation together with the anisotropic residual-based shock capturing method

Moreover, the shock upstream of the cylinder is formed as extensively described in literature (Mittal and Tezduyar, 1998). The anisotropic shock capturing method gives an accurate solution for the thin shock layer of the supersonic expansion within two or three elements. The detached shock wave presents the oblique solution for the compressible problem. It also gives correct results where gradients of the solution are not too sharp, such as for the weak tail shock that is formed in the wake structure.

5. Conclusions

In this work we have applied the variational multi-scale concept for stabilizing the compressible Navier-Stokes equations. We have presented a systematic way to design the matrix of algorithmic parameters using a Fourier analysis. We have implemented the orthogonal to the finite element space subscales, the dynamic subscales, and the non-linear tracking of subscales. The formulation have been implemented in an explicit fashion using a fourth-order RK scheme. The subsonic three-dimensional lid-driven cavity and the flow past a cylinder problems have been used to test the numerical behavior of the variational multi-scale formulation. Adequate physical solutions have been obtained, and convergence has been demonstrated for linear elements. It has been found that including the orthogonal, dynamic, and the non-linear subscales improves the accuracy of the compressible formulation. The results indicate a less-dissipative behavior of the orthogonal subscales compared to the finite element residual definition for the space of subscales.

Local instablities have been aborded with shock capturing methods. The anisotropic shock capturing method has been formulated in contrast to the isotropic method, giving better solutions for the supersonic examples. Because the anisotropic method adds the artificial diffusivity only in the crosswind direction, the non-linearity

introduced by the shock capturing method has less effect in the convergence behavior to the steady state. In order to calculate the artificial diffusion, we also proposed to use an orthogonal projection-based method, instead of the residual-based definition, with similar results.

Acknowledgments

C. Bayona acknowledges the Doctoral Scholarship received from the Colombian Goverment-Colciencias. R. Codina acknowledges the support received from the ICREA Acadèmia Program, from the Catalan Government. This work has been partially funded by the FP7 grant no. 308874 (project Eunison) and by the Ministerio de Economía y Competitividad of the Spanish Government under the Plan Nacional de Investigación 2012: AYA2012-33490. The authors thankfully acknowledges the computer resources, technical expertise and assistance provided by the Red Española de Supercomputación (RES-BSC).

Downloaded by Kungliga Tekniska Högskolan At 05:21 18 May 2016 (PT)

References

Albensoeder, S. and Kuhlmann, H.C. (2005), "Accurate three-dimensional lid-driven cavity flow", *Journal of Computational Physics*, Vol. 206 No. 2, pp. 536-558.

Baiges, J. and Codina, R. (2010), "The fixed-mesh ALE approach applied to solid mechanics and fluid-structure interaction problems", *International Journal for Numerical Methods in Engineering*, Vol. 81 No. 12, pp. 1529-1557.

Billaud, M., Gallice, G. and Nkonga, B. (2010), "Numerical mathematics and advanced applications 2009", *Stabilized Finite Element Method for Compressible-Incompressible Diphasic Flows*, Springer Berlin Heidelberg, pp. 171-179.

Brooks, A. and Hughes, T. (1981), "Streamline upwind/Petrov-Galerkin formulations for convection dominated flows with particular emphasis on the incompressible Navier-Stokes equations", *Computer Methods in Applied Mechanics and Engineering*, Vol. 32 No. 1, pp. 199-259.

Codina, R. (1993), "A discontinuity-capturing crosswind-dissipation for the finite element solution of the convection-diffusion equation", *Computer Methods in Applied Mechanics & Engineering*, Vol. 110 No. 3, pp. 325-342.

Codina, R. (2000), "Stabilization of incompressibility and convection through orthogonal sub-scales in finite element methods", *Computer Methods in Applied Mechanics & Engineering*, Vol. 190 No. 13, pp. 1579-1599.

Codina, R. (2001), "A stabilized finite element method for generalized stationary incompressible flows", *Computer Methods in Applied Mechanics & Engineering*, Vol. 190 No. 20, pp. 2681-2706.

Codina, R. (2009), "Finite element approximation of the three-field formulation of the Stokes problem using arbitrary interpolations", *SIAM Journal on Numerical Analysis*, Vol. 47 No. 1, pp. 699-718.

Codina, R. (2011), "Finite element approximation of the convection-diffusion equation: subgrid-scale spaces, local instabilities and anisotropic space-time discretizations", *BAIL 2010-Boundary and Interior Layers, Computational and Asymptotic Methods*, Springer Berlin Heidelberg, pp. 85-97.

Codina, R., González-Ondina, J.M., Díaz-Hernández, G. and Principe, J. (2008), "Finite element approximation of the modified Boussinesq equations using a stabilized formulation", *International Journal for Numerical Methods in Fluids*, Vol. 57 No. 9, pp. 1249-1268.

Codina, R., Principe, J., Guasch, O. and Badia, S. (2007), "Time dependent subscales in the stabilized finite element approximation of incompressible flow problems", *Computer Methods in Applied Mechanics & Engineering*, Vol. 196 No. 21, pp. 2413-2430.

Dahmen, W., Gotzen, T., Müller, S. and Schäfer, R. (2011), "Adaptive multiresolution finite volume discretization of the variational multiscale method", General Framework, Inst. für Geometrie und Praktische Mathematik.

Hauke, G. and Hughes, T. (1998), "A comparative study of different sets of variables for solving compressible and incompressible flows", *Computer Methods in Applied Mechanics & Engineering*, Vol. 153 No. 1, pp. 1-44.

Hauke, G., Landaberea, A., Garmendia, I. and Canales, J. (2005), "A segregated method for compressible flow computation. Part II: General divariant compressible flows", *International Journal for Numerical Methods in Fluids*, Vol. 49 No. 2, pp. 183-209.

Hughes, T. (1995), "Multiscale phenomena: Green's functions, the Dirichlet-to-Neumann formulation, subgrid scale models, bubbles and the origins of stabilized methods", *Computer Methods in Applied Mechanics & Engineering*, Vol. 127 No. 1, pp. 387-401.

Hughes, T. and Mallet, M. (1986), "A new finite element formulation for computational fluid dynamics: III. The generalized streamline operator for multidimensional advective-diffusive systems", *Computer Methods in Applied Mechanics & Engineering*, Vol. 58 No. 3, pp. 305-328.

Hughes, T., Scovazzi, G. and Tezduyar, T. (2010), "Stabilized methods for compressible flows", *Journal of Computational Science*, Vol. 43 No. 3, pp. 343-368.

Koobus, B. and Farhat, C. (2004), "A variational multiscale method for the large eddy simulation of compressible turbulent flows on unstructured meshes – application to vortex shedding", *Computer Methods in Applied Mechanics & Engineering*, Vol. 193 No. 15, pp. 1367-1383.

Kotteda, V. and Mittal, S. (2014), "Stabilized finite element computation of compressible flow with linear and quadratic interpolation functions", *International Journal for Numerical Methods in Fluids*, Vol. 75 No. 4, pp. 273-294.

Le Beau, G. and Tezduyar, T. (1991), "Finite element computation of compressible flows with the SUPG formulation", Army High Performance Computing Research Center.

Levasseur, V., Sagaut, P., Chalot, F. and Davroux, A. (2006), "An entropy-variable-based VMS/GLS method for the simulation of compressible flows on unstructured grids", *Computer Methods in Applied Mechanics & Engineering*, Vol. 195 No. 9, pp. 1154-1179.

Marras, S., Moragues, M., Vázquez, M., Jorba, O. and Houzeaux, G. (2013), "Simulations of moist convection by a variational multiscale stabilized finite element method", *Journal of Computational Physics*, Vol. 252, pp. 195-218.

Mittal, S. (1998), "Finite element computation of unsteady viscous compressible flows", *Computer Methods in Applied Mechanics & Engineering*, Vol. 157 No. 1, pp. 151-175.

Mittal, S. and Tezduyar, T. (1998), "A unified finite element formulation for compressible and incompressible flows using augmented conservation variables", *Computer Methods in Applied Mechanics & Engineering*, Vol. 161 Nos 3-4, pp. 229-243.

Polner, M. (2005), "Galerkin least-squares stabilization operators for the Navier-Stokes equations: a unified approach", University of Twente.

Rispoli, F. and Saavedra, R. (2006), "A stabilized finite element method based on SGS models for compressible flows", *Computer Methods in Applied Mechanics & Engineering*, Vol. 196 No. 1, pp. 652-664.

Rispoli, F., Corsini, A. and Tezduyar, T. (2007), "Finite element computation of turbulent flows with the discontinuity-capturing directional dissipation (DCDD)", *Computers & Fluids*, Vol. 36 No. 1, pp. 121-126.

Downloaded by Kungliga Tekniska Högskolan At 05:21 18 May 2016 (PT)

Sevilla, R., Hassan, O. and Morgan, K. (2013), "An analysis of the performance of a high-order stabilised finite element method for simulating compressible flows", *Computer Methods in Applied Mechanics & Engineering*, Vol. 253, pp. 15-27.

Shakib, F. (1989), Finite element analysis of the compressible Euler and Navier-Stokes equations.

Tezduyar, T. and Hughes, T. (1983), "Finite element analysis of the compressible Euler and Navier-Stokes equations", doctoral dissertation, Stanford University, Stanford, CA.

Tezduyar, T. and Senga, M. (2006), "Stabilization and shock-capturing parameters in SUPG formulation of compressible flows", *Computer Methods in Applied Mechanics & Engineering*, Vol. 195 No. 13, pp. 1621-1632.

Van Der Bos, F., Van Der Vegt, J. and Geurts, B. (2007), "A multi-scale formulation for compressible turbulent flows suitable for general variational discretization techniques", *Computer Methods in Applied Mechanics & Engineering*, Vol. 196 No. 29, pp. 2863-2875.

Woopen, M., Balan, A., May, G. and Schütz, J. (2014), "A comparison of hybridized and standard DG methods for target-based hp-adaptive simulation of compressible flow", *Computers & Fluids*, Vol. 98, pp. 3-16.

Corresponding author
R. Codina can be contacted at: ramon.codina@upc.edu

Downloaded by Kungliga Tekniska Högskolan At 05:21 18 May 2016 (PT)

For instructions on how to order reprints of this article, please visit our website:
www.emeraldgrouppublishing.com/licensing/reprints.htm
Or contact us for further details: **permissions@emeraldinsight.com**